

博士論文

Selective control of up-regulated and down-regulated genes

by temporal patterns and doses of insulin

(インスリン刺激の時間パターンと濃度による選択的遺伝子発現制御)

佐野 貴規

Abstract

Insulin shows postprandial transient secretion with high doses, and fasting sustained secretion with low doses, selectively controlling multiple functions. However, how temporal patterns and doses of insulin selectively control gene expression remains unknown. Here, we analyzed the temporal patterns and doses of insulin-dependent gene expression. We performed transcriptomic analysis of insulin-stimulated hepatoma FAO cells and identified 13 up-regulated insulin-responsive genes (IRGs) and 16 down-regulated IRGs. The up-regulated IRGs responded more quickly to step and pulse insulin stimulations, whereas the down-regulated IRGs showed higher sensitivity to insulin doses. Mathematical modeling revealed that signaling from insulin to transcription of the down-regulated IRGs is more rapid to insulin stimulation, whereas transcription of the up-regulated IRGs is more rapid. Furthermore, some of the IRGs were consistently up-regulated or down-regulated by insulin injection *in vivo*. Thus, our results suggest that transient high-dose insulin selectively regulates the up-regulated IRGs, whereas the sustained low-dose insulin regulates the down-regulated IRGs.

Table of Contents

1. Introduction	6
1.1 Physiological roles and time scale of insulin action.....	6
1.2 Transcriptomic responses to constant stimulations of insulin	7
1.3 Relationships between temporal patterns of stimulation and transcriptional response.....	8
1.4 Purpose of this study	9
2. Materials and Methods	11
2.1 Cell culture and insulin stimulation	11
2.2 RNA sequencing.....	12
2.3 Identification of differentially expressed transcripts	12
2.4 Identification of the IRGs by data filtering of the differentially expressed transcripts	13
2.5 Mapping of the IRGs on pathways in the KEGG database	13
2.6 Selection of the up-regulated IRGs and down-regulated IRGs	14
2.7 Quantitative reverse transcription polymerase chain reaction.....	14
2.8 Definitions of parameters for the step, pulse, ramp, and dose stimulations	15
3. Results	23
3.1 Identification of the IRGs by RNA-seq.....	23
3.2 Selection of the up-regulated and down-regulated IRGs for analysis of dynamics using qRT-PCR	24
3.3 Selective control of up-regulated and down-regulated IRGs by temporal patterns and doses of insulin.....	26
3.4 Mathematical modeling of up-regulated and down-regulated IRG expression.....	31
3.5 <i>In vivo</i> expression of up-regulated IRGs and down-regulated IRGs in the rat liver	33
4. Discussion	35
5. Figures and Figure Legends	39

Figure 1. Experimental design of insulin stimulation patterns based on <i>in vivo</i> temporal patterns of blood insulin.	39
Figure 2. Responses of the IRGs to step, pulse, and ramp stimulations and to different doses of insulin.	41
Figure 3. A pipeline for identification of the IRGs by RNA-seq.	44
Figure 4. Selection of the up-regulated and down-regulated IRGs.	46
Figure 5. The expression amounts of the up-regulated and down-regulated IRGs measured by RNA-seq and qRT-PCR.	48
Figure 6. Hierarchical clustering of expression patterns of up-regulated and down-regulated IRGs.	50
Figure 7. Hierarchical clustering by the step stimulation alone.	52
Figure 8. Responses of the IRGs to step, pulse, and ramp stimulations and the dose-responses in experiments and in simulation.	54
Figure 9. <i>In vivo</i> expression of the up-regulated IRGs and down-regulated IRGs in the rat liver.	56
Figure 10. Defining the parameters for modeling up-regulated IRGs and down-regulated IRGs from the experimental data.	57
Figure 11. Comparison of the parameters for the up-regulated IRGs and down-regulated IRGs.	60
Figure 12. Mathematical models of the pathway for the up-regulated IRGs and down-regulated IRGs.	61
Figure 13. Sensitivity and time constants of the increased and decreased IRTs from the RNA-seq data.	63
Figure 14. Analysis of response characteristics of the up-regulated and down-regulated IRGs by principal component analysis using various patterns of insulin stimulation.	67
Figure 15. Chromosome mapping and gene ontology of DEGs.	70
Figure 16. Decay time constant by pulse stimulation represents the time constant of a pathway.	72

Figure 17. Histograms of coefficient of variation (CV) of parameter values in the best 5 models among the 30 models.	75
Figure 18. Selective control of the up-regulated IRGs and down-regulated IRGs by temporal patterns and doses of insulin.....	76
Figure 19. Putative scenario of insulin action in liver.....	77
6. Tables.....	78
Table 1. Validation of Cuffdiff to identify the DEGs by changing the Cuffdiff's internal threshold (FDR).	78
Table 2. <i>q</i> values from experimental parameter comparisons between the up-regulated and down-regulated IRGs by changing the Cuffdiff's internal threshold (FDR).	79
Table 3. KEGG pathways into which five or more IRGs mapped.	80
Table 4. KEGG pathways in which the up-regulated and down-regulated IRGs were mapped.	81
Table 5. Primer sequences used for qRT-PCR measurements.	83
Table 6. Parameters of the experimental IRG responses.	85
Table 7. Up-regulated IRGs and down-regulated IRGs.....	86
Table 8. Calculated parameters from experimental qRT-PCR data.	87
Table 9. Estimated model parameters and simulated EC ₅₀ at 120 or 240 min for the up-regulated and down-regulated IRGs.....	90
7. References	91

1. Introduction

1.1 Physiological roles and time scale of insulin action

Insulin is the hormone released from β cells in the pancreas, and is the only hormone that lowers blood glucose. It also regulates systemic homeostasis via multiple cellular functions, including metabolism and gene expression (1, 2). Insulin has been reported to exhibit specific temporal patterns such as additional postprandial secretion, which is a transient high-dose secretion of insulin, and basal fasting secretion, which is sustained low-dose secretion of insulin (3, 4). Abnormalities in temporal patterns and doses of insulin secretion have been shown to be related to the pathogenesis of type 2 diabetes mellitus (4-7). Consistent with clinical observations, we have previously shown that additional pulse secretion and basal sustained secretion of insulin selectively regulate metabolic responses such as glycolysis, glycogenesis, and gluconeogenesis through the AKT-signaling pathway in FAO hepatoma cells (8, 9). We have also performed metabolomics and phosphoproteomics of acute insulin action (<60 min) and found that acute insulin action mainly involves phosphorylation and allosteric regulation rather than gene expression (10). However, the transcriptomics of insulin action, which may be particularly important for chronic insulin action (>60 min), remains to be investigated.

Temporal order of transcriptional responses to external stimuli have been grouped into three types; early, intermediate, or late response. For example, tumor necrosis factor (TNF) induces early (< 2 hours), intermediate (2 to 8 hours), and late (> 8 hours) gene expressions through oscillatory

activation of nuclear factor kappa B (NFκB) (11). As well as temporal regulation by NFκB signaling, alternative splicing is also reported to delay the transcriptional responses depending on the speed of elongation or intron removal (12). Especially, pre-mRNA of late response genes is spliced into mRNA much more slowly than the intermediate response genes, although the speeds of synthesis and degradation of pre-mRNA of those two later groups are almost equal to each other. This difference leads to the difference of the response speeds between the intermediate and late response gene groups.

As for the time span of protein expression, microorganisms have been well studied using various types of data, including transcriptome, metabolome, and proteome. Zamper et al. (13) reported that, in yeast cultured with a normal concentration of extracellular glucose, a subset of metabolic enzymes show increase in their abundances (fold change $> 2^3$) depending on activities of some transcription factors > 2 hours after glucose depletion. They also estimated the duration of the transcription activities to be up to ~ 6 hours after the glucose depletion.

1.2 Transcriptomic responses to constant stimulations of insulin

Transcriptomic analyses of insulin action over 3 to 48 hours with up to five time points and three doses in rat H4IIE hepatoma cells (14), mouse fibroblasts (15, 16), mouse osteoclast precursors (17), human skeletal muscle (18), and human placenta (19) have been reported. However, the mechanisms by which temporal patterns and doses of insulin selectively regulate gene expression have yet not

been studied. For example, Hectors *et al.* (14) evaluated dose sensitivity of the responsiveness of proliferation of and transcriptome in H4IIE cells treated with 3 doses of insulin (10 pM, 1nM, or 100 nM) for 4 time points (3, 6, 24, and 48 h). However, they did not consider rapidness of the responses. Dupont *et al.* (15) analysed a mechanism of distinct responses of signalling pathways and transcriptome to insulin and IGF-1 whose receptors are similar to each other, by treating mouse fibroblasts with 50 nM of insulin or 50 nM IGF-1 at 90 min. They just measured the response profiles and compared the responses to the different stimulations with a single dose for a single time period. They did not mention the rapidness or sensitivity to insulin. Rome *et al.* (18) studied *in vivo* transcriptomic responses to 3-h euglycemic hyperinsulinemic clamp with a single dose of insulin in skeletal muscle from healthy human bodies. Although they widely discussed biological functions of the insulin-regulated genes, they did not discuss any importances of the rapidness or sensitivity to insulin.

1.3 Relationships between temporal patterns of stimulation and transcriptional response

Behar *et al.* (20) theoretically and computationally formulated relationships between patterns of stimulation and response from signalling to gene expression under some major regulation modules. They also experimentally validated the ligand-specific responses of NFκB activity and NFκB-targeted gene expressions in response to a single dose of lipopolysaccharide or tumor necrosis factor in two temporal patterns of time course (sustained or 45-min pulse). Their approach was

outstanding but specific for NF κ B-targeted gene expression. Further analyses of stimulus-dependent transcriptomic responses remain to be elucidated. As well as the study above, because temporal patterns of growth factors and extracellular stimuli have been reported to be important for selective regulation of cellular signaling and gene expression in many cellular systems (21, 22), temporal patterns and doses of insulin are likely to differentially regulate gene expression, thereby controlling various cellular functions. It remains unknown how insulin selectively regulates global gene expression via specific temporal patterns such as additional pulse and basal sustained secretions.

1.4 Purpose of this study

To address this issue, Kentaro Kawata, Dr. Shinya Kuroda, and I conceived the project. K. Kawata analyzed the RNA sequencing (RNA-seq) data of insulin-stimulated FAO cells. K. Kawata identified 278 genes responsive to step stimulation of insulin, which we denoted as insulin-responsive genes (IRGs). Based on the functional analysis using the Kyoto Encyclopedia of the Genes and Genomes (KEGG) database, and on the experimental and statistical analyses using various temporal patterns and doses of insulin stimulations, K. Kawata and I selected 13 IRGs that showed up-regulation (up-regulated IRGs), including the key cholesterol synthesis gene *Hmgcr* [encoding 3-hydroxy-3-methylglutaryl coenzyme A (HMG-CoA) reductase], and 16 IRGs that showed down-regulation (down-regulated IRGs), including the key gluconeogenesis genes *G6pase* (encoding glucose-6-phosphatase) and *Pck1* (encoding phosphoenolpyruvate carboxykinase 1). K. Kawata, Dr.

Satoshi Ohno and I found that the up-regulated IRGs responded more quickly to step (increasing concentrations of insulin without a decrease between concentration changes) and pulse (a single transient increase in insulin concentration) stimulations of insulin than did the down-regulated IRGs, whereas the 16 down-regulated IRGs showed higher sensitivity to insulin-doses (suppressed at low concentrations of insulin). S. Ohno constructed a simple mathematical models of the IRG expressions to reveal the distinct properties of insulin signaling and transcription of the up-regulated and down-regulated IRGs. Furthermore, I validated that some of the IRGs were consistently up-regulated or down-regulated in the liver of rats by insulin injection to their portal vein. Given that additional postprandial secretion transiently occurs at a high dose and that basal fasting secretion sustainedly occurs at a low dose, our results suggested that insulin selectively exerts its postprandial action through the up-regulation of gene expressions and its fasting action through the down-regulation of gene expressions.

2. Materials and Methods

2.1 Cell culture and insulin stimulation

Rat hepatoma FAO cells were seeded at a density of 3×10^6 cells per dish on 6-cm dishes (Corning) or 1.3×10^6 cells per well on six-well plates (Iwaki) and cultured in RPMI 1640 supplemented with 10% (v/v) fetal bovine serum at 37°C under 5% CO₂ for 2 days before deprivation of serum (starvation). The cells were washed twice with ice-cold phosphate-buffered saline and starved in serum-free medium containing 0.01 nM insulin (Sigma-Aldrich) and 10 nM dexamethasone (Wako), which increases the expression of gluconeogenesis genes such as *G6pase* and *Pck1* (23), for 16 hours. 0.01 nM insulin was added before the stimulation, and 0.01 nM insulin was present throughout the experiments unless specified to mimic the *in vivo* basal secretion during fasting (Fig. 1) (4). The medium was changed at 4 and 2 hours before the stimulation. For step stimulation, the cells were stimulated by replacing the starvation medium with medium containing the specified dose of insulin and then cultured for the specified duration (Fig. 2, blue line). For pulse stimulation, the cells were stimulated by replacing the starvation medium with medium containing 10 nM insulin for 60 min, washed twice with medium without insulin, and stimulated again with medium containing 0.01 nM insulin for the remainder of the time (Fig. 2, green line). For ramp stimulation (Fig. 2, red line), the starved cells were cultured on a seesaw rocker in the incubator and stimulated by continuous addition of insulin to a maximum of 10 nM using a microsyringe pump (KD Scientific) (9).

2.2 RNA sequencing

Total RNA was extracted from FAO cells stimulated by 0.01, 1, or 100 nM insulin for 0, 15, 30, 60, 90, 120, and 240 min using RNeasy Mini Kit (Qiagen) with deoxyribonuclease I digestion to remove genomic and mitochondrial DNA. mRNA was enriched from total RNA using poly(A) selection, and the mRNA samples were validated using the 2100 Bioanalyzer (Agilent). Standard Illumina protocols were used to generate 101–base pair paired-end read libraries that were sequenced on the HiSeq 2000 platform (Illumina) (24).

2.3 Identification of differentially expressed transcripts

The sequence data of RNA-seq were analyzed using the Tuxedo suite (25). The obtained fragments were aligned to the reference genome annotation Rnor_5.0 reference (Ensembl, release 73), and junction mappings were accomplished using TopHat2 v2.0.7 (26). The FPKM values were calculated using Cufflinks (27), and the differentially expressed transcripts were identified using Cuffdiff (27). In analysis using Cuffdiff, The default value $\theta = 0.05$ was used as an internal parameter of false discovery rate (FDR). K. Kawata confirmed results of DEG selection in case the internal parameter was changed between 0.001 and 1 (Table 1), which I found partly consistent with the result with $\theta = 0.05$ (Table 2).

2.4 Identification of the IRGs by data filtering of the differentially expressed transcripts

The Otsu threshold (28) of expression value of 25.6 was calculated against all FPKM values, and the FPKM values below the threshold were substituted with zero. K. Kawata removed transcripts with FPKM = 0 through all the time points. The following transcripts were excluded: transcripts with missing points, outliers, and large expression variations. Outliers were defined as follows: if a time course had a series of three successive time points and the middle one had an FPKM value $\geq 10\%$ of the maximal FPKM value within the entire time course and the others had a value of zero, then the transcript was excluded. In addition, if a case had a time course with a series of three successive time points and the middle value was zero, whereas the others had FPKM values $\geq 10\%$ of the maximal FPKM value, then the transcript was excluded. Regarding expression variation, absolute values of the difference of the two slopes of the FPKM values at a specific time point and at an early or later time point were calculated. Considering the distribution of the calculated values, K. Kawata set a threshold of 2.57, which was three times larger than the mode of the distribution, and transcripts involving more than three time points with that threshold were excluded. The remaining 278 differentially expressed genes corresponding to 290 differentially expressed transcripts were denoted as the IRGs.

2.5 Mapping of the IRGs on pathways in the KEGG database

The IRGs were mapped on pathways in the KEGG database (29). The 278 Ensembl identifiers of the

IRGs corresponding to 290 IRTs were related to 203 KEGG gene identifiers using Ensembl BioMart (release 75) (30). Mapping the IRGs to the KEGG pathways was done using the KEGG mapper tool (www.kegg.jp/kegg/mapper.html). Pathways with five or more IRGs were extracted (Tables 3 and 4).

2.6 Selection of the up-regulated IRGs and down-regulated IRGs

K. Kawata selected IRTs corresponding to the IRGs mapped on the KEGG pathways that showed sustained increased or decreased responses at 120 and 240 min and classified them into three groups on the basis of their expression patterns: the up-regulated IRTs, the down-regulated IRTs, and the other IRTs (Figs. 3A and 4A). For the classification of the expression patterns, K. Kawata calculated a mean of CVs of the IRT responses to 0.01 nM insulin and set a threshold, the mean + 2σ (0.494). IRTs with a CV value greater than the threshold were classified as the other IRTs. Among the IRTs with a CV value less than or equal to the threshold, for cases in which FPKM values for 1 and 100 nM insulin stimulation at 120 and 240 min were greater or less than those for 0.01 nM, the IRTs were classified into up-regulated or down-regulated IRTs. The rest of the IRTs were classified as the other IRTs (Fig. 4).

2.7 Quantitative reverse transcription polymerase chain reaction

qRT-PCR was performed as previously described (8). Briefly, total RNA was extracted from FAO

cells using RNeasy Mini Kit (Qiagen) and reverse-transcribed into complementary DNA (cDNA) using the High-Capacity RNA-to-cDNA Kit (Applied Biosystems) according to the manufacturer's protocol. The cDNA samples were amplified using the Power SYBR Green PCR Master Mix (Applied Biosystems) and the 7300 Real-Time PCR system (Applied Biosystems) according to the manufacturer's protocol. The primer sequences used in the qRT-PCR analysis are listed in Table 5. The fold changes were calculated on the basis of the $\Delta\Delta C_t$ method (Figs. 2, 5, 6, 7, 8, and 9) using the expression of *36B4* as a reference gene.

2.8 Definitions of parameters for the step, pulse, ramp, and dose stimulations

I defined the parameters that characterize the response rates and amplitudes by the pulse and ramp stimulation of insulin and the sensitivity to insulin dose responses (Fig. 10 and Table 6). The fold change over the 0-min time point was used for estimating the parameters from experiments. For the step stimulation, *Time_Constant_Step* was defined as the time when the response first reached 50% of the peak amplitude ($1/2$ *Peak_Step*). *Time_Constant_Step* was calculated on the basis of linear interpolation. For pulse stimulation, *Time_Peak_Pulse* was defined as the time when the amplitude of the response reached the maximum (*Peak_Pulse*). *Time_Decay_Pulse* was defined as the decay time when the decayed response reached 50% of the *Peak_Pulse*. The *Time_Decay_Pulse* was calculated on the basis of linear interpolation. *Ratio_240min_Pulse* was defined as the ratio of the amplitude at 240 min by the pulse stimulation (*240min_Pulse*) to that by the step stimulation

(240min_Step). For ramp stimulation, Time_Constant_Ramp was defined as the time when the amplitude reached 50% of the maximal amplitude (1/2 Peak_Ramp). The Time_Constant_Ramp and the Time_Constant_contStep_Ramp were calculated on the basis of linear interpolation. Ratio_120min_Ramp was defined by the ratio 120min_Ramp/120min_Step. Ratio_180min_Ramp was defined as the ratio 180min_Ramp/180min_Step. Ratio_240min_Ramp was defined as the ratio 240min_Ramp/240min_Step. For the dose responses at 120 and 240 min, four parameters, EC_{50} , b , n , and V_{max} , were defined on the basis of modification of the Hill function as follows:

$$\begin{cases} y = b + \frac{V_{max} Dose^n}{Dose^n + EC_{50}^n} & \text{(for up-regulated IRGs),} \\ y = (b - V_{max}) + \frac{V_{max} Dose^n}{Dose^n + EC_{50}^n} & \text{(for down-regulated IRGs),} \end{cases}$$

where Dose, n , EC_{50} , b , and V_{max} represent the dose of insulin, the apparent Hill's coefficient, the apparent half-maximal effective concentration, and the lower limit and the upper limit of the dose-response curve, respectively. These parameters were estimated so the y values fitted the experimental data using MATLAB (version R2014a, MathWorks) based on the simplex search method (31) to minimize the residual sum of squares (RSS) between y and the experimental data.

2.9 Wilcoxon rank-sum test

Statistical comparisons of the medians of the parameters between the up-regulated and down-regulated IRGs were performed using Wilcoxon rank sum test. P values were adjusted for multiple testing with the Benjamini-Hochberg correction (32) using MATLAB function mafdr, and

the adjusted P values are shown as q values. Data are shown as median with quartiles (Figs.11, 12B and 13C).

2.10 Hierarchical clustering of IRGs using qRT-PCR data

I performed hierarchical clustering of the responses of the up-regulated or down-regulated IRGs to all stimulation patterns or step stimulation (10 nM) alone (Figs. 6 or 7, respectively). The data were normalized in advance as follows. For the 16 sustained increased IRGs or 18 sustained decreased IRGs, the data were arranged as matrices of the log₂ fold change of 43 or 8 time points for all the stimulation patterns or the step stimulation alone, respectively. The M -by- N data matrix composed of the N time points of the M IRGs ($M < N$) was normalized by scaling the variation to 1 in the row direction and averaged to 0 in both the row and column directions:

$$x'_{ij} = \frac{x_{ij}}{s_i} - \frac{1}{M} \sum_i \left(\frac{x_{ij}}{s_i} \right) - \frac{1}{N} \sum_j \left(\frac{x_{ij}}{s_i} \right) + \frac{1}{MN} \sum_i \sum_j \left(\frac{x_{ij}}{s_i} \right)$$

where s_i , x_{ij} , and x'_{ij} represent the standard deviation (SD) at the i th row of the raw matrix, the element of the raw matrix at the i th row and at the j th column, and the element of the normalized matrix at the i th row and at the j th column, respectively. I next implemented the hierarchical clustering using the Euclidean distance for calculation of the intracluster distances and using Ward's method for calculation of the intercluster distances (Figs. 6 and 7).

2.11 Principal component analysis of the up-regulated and down-regulated IRG responses

using various patterns of insulin stimulation

I conducted principal component (PC) analysis using the qRT-PCR data containing fold change over 0 min of both the up-regulated and down-regulated IRGs in response to all the patterns of insulin stimulation (Fig. 14). The raw data matrix (\mathbf{X}_0) containing 29 genes for 43 time points from all the stimulation patterns were normalized in the same way as **2.10**. Considering the effect of each principal component to the expression patterns, the M -by- N normalized data matrix \mathbf{X}' ($M < N$) was decomposed by singular value decomposition as follows:

$$\mathbf{X}' = \mathbf{T}\mathbf{V}^T = \mathbf{U}\mathbf{D}\mathbf{V}^T = \sum_{j=1}^M \mu_j \mathbf{u}_j \mathbf{v}_j^T = \mu_1 \mathbf{u}_1 \mathbf{v}_1^T + \mu_2 \mathbf{u}_2 \mathbf{v}_2^T + \cdots + \mu_M \mathbf{u}_M \mathbf{v}_M^T,$$

where the matrices \mathbf{T} and \mathbf{V} represent the score matrix and the loading matrix, respectively, and where μ_j represents the j th singular value, \mathbf{u}_j and \mathbf{v}_j represent the j th eigenvector in the matrices \mathbf{U} and \mathbf{V} , respectively. The two matrices \mathbf{U} and \mathbf{V} satisfy the following:

$$\begin{aligned} \mathbf{X}'(\mathbf{X}')^T &= \mathbf{U}\mathbf{D}^2\mathbf{U}^T = \sum_{j=1}^M \mu_j^2 \mathbf{u}_j \mathbf{u}_j^T \\ (\mathbf{X}')^T \mathbf{X}' &= \mathbf{V}\mathbf{D}^2\mathbf{V}^T = \sum_{i=1}^M \mu_i^2 \mathbf{v}_i \mathbf{v}_i^T. \end{aligned}$$

By the way, the normalized matrix \mathbf{X}' is also expressed as follows:

$$\mathbf{X}' = \mathbf{X} - \bar{\mathbf{m}}_M - \bar{\mathbf{m}}_N + \bar{\mathbf{m}}_{MN} = \mathbf{X} - \bar{\mathbf{m}} \quad (\bar{\mathbf{m}} := \bar{\mathbf{m}}_M + \bar{\mathbf{m}}_N - \bar{\mathbf{m}}_{MN}),$$

where \mathbf{X} is an M -by- N matrix with its variances in the row direction scaled to 1, and where $\bar{\mathbf{m}}_M$, $\bar{\mathbf{m}}_N$, and $\bar{\mathbf{m}}_{MN}$ are M -by- N matrices consisting mean values of the scaled matrix \mathbf{X} in the row, column, and row-and-column directions, respectively, i.e.:

$$\bar{\mathbf{m}}_M := \begin{pmatrix} m_{1.} & m_{1.} & \cdots & m_{1.} \\ m_{2.} & m_{2.} & \cdots & m_{2.} \\ \vdots & \vdots & \ddots & \vdots \\ m_{M.} & m_{M.} & \cdots & m_{M.} \end{pmatrix}, \bar{\mathbf{m}}_N := \begin{pmatrix} m_{.1} & m_{.2} & \cdots & m_{.N} \\ m_{.1} & m_{.2} & \cdots & m_{.N} \\ \vdots & \vdots & \ddots & \vdots \\ m_{.1} & m_{.2} & \cdots & m_{.N} \end{pmatrix}, \bar{\mathbf{m}}_{MN} := \begin{pmatrix} m & m & \cdots & m \\ m & m & \cdots & m \\ \vdots & \vdots & \ddots & \vdots \\ m & m & \cdots & m \end{pmatrix},$$

where $m_{i.}$ and $m_{.j}$ are the mean values of the scaled matrix \mathbf{X} in the row and column directions, respectively, and where m is a mean value of all the elements of the scaled matrix \mathbf{X} . So, the raw data matrix \mathbf{X}_0 is decomposed as follows:

$$\begin{aligned} \mathbf{X}_0 &= \mathbf{X} * \mathbf{s}_M \\ &= \left(\bar{\mathbf{m}} + \sum_{j=1}^M \mu_j \mathbf{u}_j \mathbf{v}_j^T \right) * \mathbf{s}_M, \\ &= \bar{\mathbf{m}} * \mathbf{s}_M + \mu_1 \mathbf{u}_1 \mathbf{v}_1^T * \mathbf{s}_M + \mu_2 \mathbf{u}_2 \mathbf{v}_2^T * \mathbf{s}_M + \cdots + \mu_M \mathbf{u}_M \mathbf{v}_M^T * \mathbf{s}_M \end{aligned}$$

where “*” means here an operation of multiplication with respect not to 2 matrices but to each element of 2 matrices, and where \mathbf{s}_M is an M -by- N matrix consisting of standard deviations of the raw data matrix \mathbf{X}_0 in the row direction, i.e.:

$$\mathbf{s}_M := \begin{pmatrix} s_{1.} & s_{1.} & \cdots & s_{1.} \\ s_{2.} & s_{2.} & \cdots & s_{2.} \\ \vdots & \vdots & \ddots & \vdots \\ s_{M.} & s_{M.} & \cdots & s_{M.} \end{pmatrix},$$

where $s_{i.}$ is a standard deviation in the i th row direction in the raw data matrix \mathbf{X}_0 .

In order to capture the variance of each principal component, I illustrated the decomposed gene expression profiles: the mean component ($\bar{\mathbf{m}} * \mathbf{s}_M$) and the principal components 1 to 3 ($\mu_j \mathbf{u}_j \mathbf{v}_j^T * \mathbf{s}_M$ ($j=1, 2, 3$)) (Fig. 14F).

2.12 Mathematical model and parameter estimation

Mathematical models of insulin-dependent IRG expression in Fig. 12 were constructed as follows:

$$\frac{dx}{dt} = \frac{V_{\max 1} I}{K_{M1} + I} - k_1 x$$

$$\begin{cases} \frac{dm}{dt} = \frac{V_{\max 2} x}{K_{M2} + x} - k_2 m, & \text{if } m \text{ is from up-regulated IRGs} \\ \frac{dm}{dt} = \frac{V_{\max 2} K_{M2}}{K_{M2} + x} - k_2 m, & \text{if } m \text{ is from down-regulated IRGs} \end{cases}$$

where I , x , and m stand for concentration of insulin, insulin signalling-dependent transcriptional regulator, and mRNA of the IRGs, respectively. The former equation can be regarded as signaling from insulin to the nucleus (insulin signaling), and the latter equations can be regarded as the transcription including synthesis and degradation of the IRTs. The initial values of x were calculated by assuming equilibrium of x , and the initial values of m were set to mean values of experimental qRT-PCR measurements from step, pulse, and ramp stimulations of 10 nM insulin at 0 min. $V_{\max 2}$ is calculated by assuming equilibrium of m at 0 min. Therefore, the remaining parameters to be estimated are k_1 , K_{M1} , k_2 , K_{M2} , and $V_{\max 1}$.

The parameters of k_1 , K_{M1} , k_2 , K_{M2} , and $V_{\max 1}$ for each IRG were estimated to reproduce the mRNA time course by minimizing the RSS error:

$$\text{RSS} = \sum (m - m_{\text{exp}})^2$$

where m_{exp} is the normalized time course of experimental mRNA amounts by step, pulse, ramp, or dose stimulation of insulin. For each IRG, the data comprised 42 data points consisting of eight time points by step, pulse, or ramp stimulation and two time points from nine doses. Before estimation, the experimental step data were normalized by dividing them by their Euclidean norm, and the pulse,

ramp, or dose data were divided by the Euclidean norm of qRT-PCR measurements from step stimulation of 10 nM insulin, which were measured on the same day as the corresponding experiments.

The minimization problem of RSS was numerically solved by an evolutionary programming method to approach the local minimum using COPASI (complex pathway simulator) (33) on MATLAB, followed by application of the interior point method to reach the local minimum using MATLAB function `fmincon`. The numbers of parents and generations in the meta-evolutionary program were 200 and 2000, respectively. Parameter estimation was performed 30 times for each IRG to obtain the best parameter sets with minimized RSS. The ordinary differential equations of x by step or pulse stimulation were solved analytically, and the others were solved using MATLAB function `ode15s`. All simulations were performed using MATLAB (version R2014a, MathWorks) on a Windows machine or on the super computer system of National Institute of Genetics Research Organization of Information and Systems.

2.13 *In vivo* insulin injection (insulin clamp)

All rat studies were approved by the Kyushu University Institutional Animal Care and Use Committee. Ten-week-old male Sprague-Dawley rats were purchased from Japan SLC Inc. After overnight fasting, rats were anesthetized by isoflurane. To suppress endogenous insulin secretion, somatostatin was administered through the jugular vein (3 $\mu\text{g}/\text{kg}$ per min). Insulin was administered

through the mesenteric vein at the indicated dose, maintaining the blood glucose concentration at a constant amount (150 mg/dl) (Fig. 9A). Blood was sampled at the indicated time points, and blood insulin amounts were measured using a rat insulin enzyme-linked immunosorbent assay kit (Shibayagi Co. Ltd.) (Fig. 9A). At the indicated time points, the rats were killed, and the livers were immediately frozen with liquid nitrogen (34). The livers were harvested, and total RNA was isolated using RNeasy Mini Kit (Qiagen). Total RNA was reverse-transcribed into cDNA using the QuantiTect Reverse Transcription Kit (Qiagen) according to the manufacturer's protocol.

3. Results

3.1 Identification of the IRGs by RNA-seq

K. Kawata identified the IRGs and characterized those that were up-regulated and down-regulated according to the procedures shown in Fig. 3. We performed RNA sequencing (RNA-seq) with the mRNA samples from insulin-stimulated rat hepatoma FAO cells (Fig. 3A). K. Kawata mapped the fragment sequences obtained from RNA-seq to the rat genome using TopHat (22, 23), an alignment software package in the Tuxedo suite (22). K. Kawata calculated values for fragments per kilobase of exon per million mapped fragments (FPKM) for each sample by using Cufflinks (24), a program in the Tuxedo suite for transcript assembly and abundance estimation, and acquired 29,165 time courses of the transcripts. The FPKM values of the samples stimulated by 1 or 100 nM insulin at each time point for each transcript were compared to those of the control (0.01 nM insulin) by using Cuffdiff (24). Four hundred ninety transcripts and 437 corresponding genes were identified as differentially expressed transcripts (DETs) and differentially expressed genes (DEGs), respectively. Among them, the DETs whose expression patterns had missing point(s), outlier(s), and zig-zag pattern(s) were filtered out (Fig. 1B), and 290 DETs and 279 corresponding DEGs were selected as insulin-responsive transcripts (IRTs) and IRGs, respectively (Fig. 1A; see Materials and Methods).

3.2 Selection of the up-regulated and down-regulated IRGs for analysis of dynamics using qRT-PCR

K. Kawata conducted functional analysis of the IRGs using the Kyoto Encyclopedia of the Genes and Genomes (KEGG) database (29). K. Kawata searched the database for the pathway IDs of the 203 IRGs and extracted 170 KEGG pathways in which 97 of the 203 IRGs were mapped. K. Kawata selected 12 KEGG pathways where five or more IRGs were mapped (Tables 3 and 4). The 12 pathways contained 53 IRGs and 55 corresponding IRTs (Figs. 3A and 4B; Tables 3 and 4; data file S1, which can be downloaded from <http://stke.sciencemag.org/content/9/455/ra112>). Of the 12 pathways, “Metabolic pathways” (KEGG Pathway ID: rno01100) involved 14 IRGs, which was the largest number (15 IRTs). “MAPK signaling pathway” (KEGG Pathway ID: rno04010) involved 12 IRGs, which was the second largest number (12 IRTs). Both “PI3K-Akt signaling pathway” (KEGG Pathway ID: rno04151) and “Bile secretion” (KEGG Pathway ID: rno04976) included seven IRGs, which was the third largest number (seven IRTs). Thus, the pathways where the IRGs were assigned are consistent with the known functions of insulin signaling, indicating that at least these 53 IRGs were good candidates for proceeding to the next steps in identifying the best IRGs for investigating temporal and dose effects of insulin signaling in liver cells. The IRGs included some of the immediate-early genes, such as *Egr1*, *Egr2*, *c-Jun*, *JunB*, and *JunD*, which were removed from the data set by the selection process using the KEGG database. This left 290 DETs and 278 corresponding DEGs as insulin-responsive transcripts (IRTs) and IRGs, respectively (Fig. 3A; see

data file S1, which can be downloaded from <http://stke.sciencemag.org/content/9/455/ra112>).

To extract IRGs exhibiting consistent and reproducible up-regulation or down-regulation for subsequent analyses on rapidness and sensitivity, I performed additional filtering of the 53 IRGs. From the 53 IRGs, I excluded the IRGs that highly exhibited variable expression under the control (0.01 nM insulin) condition (Fig. 4A; see Materials and Methods) from further study. We excluded from further study the IRGs whose expression level of the control (0.01 nM insulin) was highly variable (Fig. 4A; see Materials and Methods). Because most of the other IRGs showed a sustained increase or decrease, we selected those whose expression at 120 and 240 min with 1 and 100 nM insulin stimulations were higher and lower than those of the control (0.01 nM insulin), respectively (Figs. 3A and 4A). We tried to confirm the expression of the selected IRGs by qRT-PCR analyses (Fig. 5 and Table 5). Many of them showed Pearson correlation coefficients greater than 0.7. Of the sustained increased IRGs, I excluded *Ppp3r1* from analysis because I could not obtain primers for detecting isoform-specific expression. I also excluded *Serpine1* because I could not detect its expression by qRT-PCR. Although examined under different stimulation conditions that were used here, I included four up-regulated IRGs (*Actb*, *Msmol*, *Rassf1*, and *Zyx*) and two down-regulated IRGs (*G6pase* and *Pck1*) that were reportedly regulated in insulin-stimulated H4IIE hepatoma cells (Table 7) (14). At the end of the filtering process, 16 sustained increased IRGs and 18 sustained decreased IRGs were selected, and confirmed by RNA-seq and qRT-PCR analyses. Hereafter, I used

qRT-PCR for the analysis of the IRGs exhibiting a sustained increase or decrease. These genes do not include some notable genes that are known to play critical roles in insulin action, including *glucokinase*, whose product catalyzes phosphorylation of glucose. In this study, *glucokinase* might have been filtered out in the process of RNA-seq analysis because the gene was not mapped to “Metabolic pathways” in the KEGG database.

In order to investigate functions of the DETs, K. Kawata searched for specific chromosomal regions where DETs were expressed in response to insulin using Ensembl database and Integrative Genomics Viewer (IGV) tool (35). As a result, significantly expressed region was not found on the rat chromosomes (Fig. 15A). Also, enrichment analysis using Biological Network Gene Ontology (BiNGO) tool (36) showed no notable terms (Fig. 15B).

3.3 Selective control of up-regulated and down-regulated IRGs by temporal patterns and doses of insulin

To examine how the expression of these genes responded to different patterns and doses of insulin that were similar to conditions *in vivo*, I applied pulse stimulation with high doses of insulin to mimic the transient increase that occurs after a meal and ramp stimulation with low doses of insulin to mimic basal insulin concentrations that would accumulate during an overnight fast (Figs. 1 and 2A). To generate a dose-response curve, I also performed step increases in insulin concentration and measured the response either 120 or 240 min after increasing the dose (Fig. 2A). For the pulse

stimulation, the cells were placed in 0.01 nM insulin and then the concentration of insulin was increased to 10 nM for 60 min and the medium was returned to 0.01 nM insulin. For the ramp stimulation, I linearly increased the amount of insulin in the medium from 0.01 to 10 nM over the course of 4 hours. I monitored the change in expression of the IRGs over the 4-hour time course.

I performed an initial screen, and cluster analysis revealed three main groups for the up-regulated IRGs (Fig. 6, A and B, and data files S3 to S5, which can be downloaded from <http://stke.sciencemag.org/content/9/455/ra112>). Although cluster U3 (*Cxcl1*, *Dusp5*, and *Ppp1r3b*) showed the strongest response in the averaged amplitude for the IRGs with a sustained increase, I eliminated these from further analysis or inclusion in the model because the response of this cluster to the control (0.01 nM insulin) medium change was greater than twofold (Fig. 6B). The down-regulated IRGs also clustered into three groups (Fig. 6, C and D), and I excluded cluster D3 (*Amacr* and *Cflar*) from the 18 IRGs with a sustained decrease because this cluster showed no significant response to high doses of insulin (Fig. 6D). After this initial screen, I had 13 IRGs in the sustained increase group and 16 IRGs in the sustained decrease group (Table 7 and Fig. 4B), including those from the previous study (14), and hereafter denoted as the up-regulated and down-regulated IRGs. The up-regulated IRGs include genes encoding proteins involved in lipid synthesis, such as *Hmgcr*, which encodes a key enzyme involved in the key cholesterol synthesis (Table 4) and has previously been reported to be stimulated by insulin (37). The down-regulated IRGs include those encoding proteins involved in gluconeogenesis, such as *G6pase* and *Pck1* (Table

4), which have previously been reported to be suppressed by insulin (38, 39).

I repeated the step, pulse, and ramp stimulations and the steps with increasing doses of insulin (Fig. 2A) with three biologically independent experiments and examined the responses of the up-regulated and down-regulated IRGs (Figs. 2B and 8, Table 6, and data file S2, which can be downloaded from <http://stke.sciencemag.org/content/9/455/ra112>). To quantitatively evaluate the responses of the up-regulated and down-regulated IRGs, I defined the parameters that characterize time constants and peak amounts of the transient and the sustained responses for each up-regulated and down-regulated IRG (Fig. 10A and Tables 6 and 8). The time constants represent the inverse of the rate of the response, and the peak amounts indicate the amplitudes of the response. I assumed that the time constant for the pulse stimulation represented the time constant of the “pathway,” with the pathway defined as a first-order, linear time-invariant system (Fig. 16). I also calculated the ratio of fold change of the sustained response between the step and pulse stimulation conditions and between the step and ramp stimulation conditions (Fig. 10A). For the dose-response data, I evaluated the responses of the up-regulated and down-regulated IRGs at 120 and 240 min of the step stimulation and defined the parameters that represented the sensitivity to insulin: Hill’s coefficient, half-maximal effective concentration (EC_{50}), V_{max} , and b (Fig. 10B and Tables 6 and 8). To determine whether the up-regulated and down-regulated IRGs exhibited different responses to insulin, I compared the medians of the parameters for each of the stimulation conditions. Significant differences were found in some of the parameters between the up-regulated and down-regulated IRGs (Fig. 11, A to D).

Compared with the down-regulated IRGs, the up-regulated IRGs had significantly smaller time constants under the step stimulation (Fig. 11A). The up-regulated IRGs had significantly smaller time constants under the pulse stimulation (Fig. 11B, Time_Decay_Pulse) and a significantly smaller ratio of fold change of sustained response at 240 min between the step and pulse stimulation conditions (Fig. 11B, Ratio_240min_Pulse) than the down-regulated IRGs. These two parameters characterized how the degradation or removal of insulin affects the rate of the response. Collectively, these results indicated that the up-regulated IRGs responded more rapidly to step or pulse stimulation than did the down-regulated IRGs.

By evaluating the sensitivity parameters, I determined that the EC_{50} values at 120 and 240 min for the down-regulated IRGs were significantly smaller than those of the up-regulated IRGs (Fig. 11D), indicating that down-regulated IRGs had higher sensitivity (151 and 137 pM at 120 and 240 min, respectively) to insulin concentration than the up-regulated IRGs (88.4 and 13.3 nM at 120 and 240 min, respectively). Furthermore, the Hill's coefficient was higher for the down-regulated IRGs, indicating that overall cooperative action by insulin signaling and transcriptional regulation in down-regulated IRGs is larger than that in up-regulated IRGs, and the V_{max} at both 120 and 240 min was higher for the up-regulated IRGs (Fig. 11D).

Thus, up-regulated IRGs responded more rapidly to the step and pulse stimulation than did down-regulated IRGs. Down-regulated IRGs showed higher sensitivity than up-regulated IRGs. These results indicated that the expressions of the up-regulated IRGs and down-regulated IRGs were

differentially affected by the temporal patterns and doses of insulin.

To determine whether this differential responsiveness was a general property of IRTs, I applied step stimulation from 0.01 to 1 to 100 nM and calculated the sensitivities and time constants of the other IRTs (Fig. 13 and data file S6, which can be downloaded from <http://stke.sciencemag.org/content/9/455/ra112>), including the 70 that increased and the 87 that decreased among the 290 IRTs. This larger cohort of IRTs exhibited a similar significant difference between the increased and decreased IRTs; the increased IRTs had lower sensitivity at 120 and 240 min and faster time constant in response to each of the two concentrations of insulin stimulation (Fig. 13 and data file S6), suggesting that these differences in responsiveness may be a general property of IRGs.

In addition, to confirm the consistency of the parameter differences between the up-regulated and down-regulated IRGs by changing the internal threshold (FDR) of Cuffdiff, K. Kawata changed the threshold between 0.001 and 1, repeated identification of the DEGs (Table 1). The smaller FDR threshold I used, the less DEGs were identified. Six (*Zyx*, *Gadd45a*, *Epha2*, *Actg1*, *Srf*, and *Rassf1*) out of the 13 up-regulated IRGs were consistently identified with the threshold = 0.001. Six (*Pck1*, *Irs2*, *Ccng2*, *Lpin1*, *Nr0b2*, and *G6pase*) out of the 16 down-regulated IRGs were consistently identified with the threshold = 0.001.

As well as identification of the DEGs, I calculated the experimental parameters (Table 8) from qRT-PCR data (Figs. 2 and 8) by changing the threshold between 0.001 and 1. The smaller FDR

threshold I used, the less parameters were significantly different. Only Ratio_240min_Pulse, which characterizes the rapidness of the IRG response, was significantly different even under the threshold = 0.001. On the other hand, parameters of the sensitivity to insulin had consistently significant differences between the up-regulated and down-regulated IRGs under any threshold except for 0.01. These results suggest conclusion of this study might have generality.

3.4 Mathematical modeling of up-regulated and down-regulated IRG expression

To gain insight into what steps in signaling pathway may control selective regulation of IRG expression, S. Ohno constructed simple mathematical models of the up-regulated and down-regulated IRG expressions (Fig. 12A). The model consists of two parts: (i) signaling from insulin to the nucleus, which I consider to end at transcription (insulin signaling), and (ii) transcription, which I consider to include synthesis and degradation of the IRTs (Fig. 12A). To determine the parameters on which the model was most dependent, I quantified the coefficient of variation (CV) in the best five models among the 30 models obtained during parameter estimation process (see Materials and Methods). The parameter values k_1 , k_2 , and K_{M1} had relatively smaller CVs than K_{M2} and V_{max1} (Fig. 17). Therefore, I analyzed k_1 , k_2 , and K_{M1} . Note that the rate constants k_1 and k_2 (Fig. 12A) are the inverse of time constants and characterize the rapidness of the pathway (Fig. 16). I plotted the simulated time courses of the up-regulated and down-regulated IRGs onto the experimental results (Figs. 2 and 8). For the first part of the model that represents insulin signaling,

the calculated rate constants (k_1) of the down-regulated IRGs are significantly larger than those of the up-regulated IRGs (Fig. 12B). Therefore, the model showed that the insulin signaling part of the process for the down-regulated IRGs is more rapid to insulin stimulation than this part of the process is for the up-regulated IRGs. For the transcription part of the process, the degradation rate constants of transcription (k_2) of the up-regulated IRGs are significantly larger than those of the down-regulated IRGs (Fig. 12B), indicating that transcription of the up-regulated IRGs occurs more rapidly than that of the down-regulated IRGs. This suggests that the more rapid time constants of the up-regulated IRGs in response to the step and pulse stimulation (Figs. 11, A and B, and 12B, and Tables 8 and 9) depend on a more rapid rate of transcription rather than a more rapid rate of insulin signaling. Furthermore, the rapid degradation rate for the messages is consistent with the ability to respond to transient signals.

The EC_{50} values at 120 and 240 min of the down-regulated IRGs in both the experiment and the mathematical model are significantly smaller than those of the up-regulated IRGs (Figs. 11D and 12B and Tables 8 and 9). Together, these results indicate that the insulin signaling part of signal transmission for the down-regulated IRGs is more rapid than that for the up-regulated IRGs, whereas transcription for the up-regulated IRGs is more rapid than that for the down-regulated IRGs. In addition, these results suggested that the difference in rate of the response to pulse stimulation (Time_Decay_Pulse and Ratio_240min_Pulse) between the up-regulated and down-regulated IRGs is derived from differences in the rate of transcription. The model could not capture the downward

trend of some of the up-regulated IRGs by the step and pulse insulin stimulations. This is partly because of the limitation of the model structure in which the downward trend cannot be reproduced by the step stimulation regardless of the parameters. In case an IRG is regulated by a few preceding gene expressions, such IRG may be expressed or suppressed in an insulin-dependent manner. Although addition of an insulin-dependent suppression of mRNA to the model structure may improve the fitting results, it will bring another difficulty in considering the number of the preceding gene expression processes. Further study is necessary to address this issue.

3.5 *In vivo* expression of up-regulated IRGs and down-regulated IRGs in the rat liver

I next examined the *in vivo* expression of up-regulated and down-regulated IRGs by insulin injection (insulin clamp) in the rat liver (Fig. 9A and data file S7, which can be downloaded from <http://stke.sciencemag.org/content/9/455/ra112>). Four of the 13 up-regulated IRGs, including *Hmgcr*, were up-regulated by insulin injection (Fig. 9B, Table 7, and data file S8, which can be downloaded from <http://stke.sciencemag.org/content/9/455/ra112>). Five of the 16 down-regulated IRGs, including *G6pase*, *Pck1*, and *Ehhadh*, were down-regulated by insulin injection (Fig. 9B, Table 7, and data file S8). Notably, *Hmgcr*, the key gene for cholesterol synthesis, was consistently up-regulated, and *G6pase* and *Pck1*, key genes for gluconeogenesis, were consistently down-regulated in the rat liver in response to insulin injection. Although the rest of the IRGs did not show statistically significant responses to insulin injection *in vivo*, other doses of insulin or examination at other time points may

identify insulin-dependent changes in expression.

4. Discussion

We demonstrated selective control of gene expression by temporal patterns and doses of insulin (Fig. 18). It has been reported that the additional postprandial secretion of insulin shows a transient temporal pattern at a high dose (approximately on the order of nano-molar with a duration of approximately 3 hours), and that basal fasting secretion shows a sustained temporal pattern at a low dose [approximately on the order of tens of pico-molar with a duration of approximately 10 hours (overnight fasting)] (Fig. 1) (4). In our experiments, the medians of the EC_{50} values of the up-regulated IRGs are 88.4 nM at 120 min and 13.3 nM at 240 min, whereas those of the down-regulated IRGs are 151 pM at 120 min and 137 pM at 240 min (Fig. 11D and Table 8), suggesting that the down-regulated IRGs can respond to the basal secretion but that the up-regulated IRGs do not. The medians of decay time by pulse stimulation (Time_Decay_Pulse) of the up-regulated and down-regulated IRGs, which may correspond to the apparent time constant of the overall pathway from stimulation to gene expression (Figs. 11B and 13, and Table 8) (40), were 178 and 240 min, respectively. In general, when the duration of stimulation is longer than the time constant of a biochemical pathway, downstream molecules can efficiently respond to the stimulation; however, when the duration of stimulation is shorter than the time constant of a biochemical pathway, downstream molecules cannot efficiently respond (40). Given that the duration of additional secretion (approximately 3-h duration) is longer than the time constant of the up-regulated IRGs (178 min) and shorter than that of the down-regulated IRGs (240 min), the up-regulated IRGs rather than

the down-regulated IRGs, are likely to efficiently respond to the additional secretion. Taken together, these results suggest that the up-regulated IRGs mainly respond to the additional insulin secretion during the postprandial period, whereas the down-regulated IRGs mainly respond to basal insulin secretions that occur during fasting.

The up-regulation or down-regulation of the IRGs we selected was consistent with previous reports and with the known functions of the encoded products. We have previously shown that additional secretion-like pulse stimulation induces transient activation of S6 kinase and production of fructose 1,6-bisphosphate and glycogen, whereas basal secretion-like ramp stimulation with a low dose of insulin induces sustained suppression of *G6pase* and *Pck1* (8, 9). The responses of the down-regulated IRGs *G6pase* and *Pck1* are consistent with the previous observations (38, 39) and with the known functions of the encoded products in gluconeogenesis, suggesting that the rest of the down-regulated IRGs can similarly respond to basal secretion. Insulin also inhibits fatty acid catabolism (41), and we identified *Ehhadh*, which encodes a metabolic enzyme associated with β -oxidation, as a down-regulated IRG, suggesting that β -oxidation in fatty acid catabolism is regulated by insulin through the suppression of gene expression. Taken together, our results suggest a mechanism of insulin-dependent suppression of fatty acid catabolism via down-regulation of *Ehhadh*. These IRGs were consistently down-regulated in response to insulin in the liver (Fig. 9B and Table 7). Postprandial insulin secretion has been reported to promote cholesterol biosynthesis (42, 43). In support of this, we identified *Hmgcr*, whose product, HMG-CoA reductase, is a key enzyme

of cholesterol biosynthesis as an up-regulated IRGs, which is also consistent with the previous report (37). This IRG was consistently up-regulated in response to insulin in the liver (Fig. 9B and Table 7). Our results also suggest a mechanism of enhancement of cholesterol synthesis in response to the additional secretion of insulin. Functional clustering of the up-regulated and down-regulated IRGs may give us insight in a well understanding of insulin action.

In this study, we selected the IRGs that showed sustained up-regulation or down-regulation because most of the DEGs showed such dynamics. According to previous reports about the temporal order of transcriptomic dynamics (12, 35), the profiles are generally clustered into main three groups. So, improvement of our experimental and analytical procedures may allow us to detect the other types of transcripts, including early response genes and intermediate response genes, depending on the experimental procedures such as additional time points or doses, additional measurements such as chromatin immunoprecipitation sequencing (ChIP-seq). Also, we used several patterns of insulin stimulation in this study, and found it useful to cluster the expression dynamics of gene expression. Using temporally modified stimulations can be also a clue to detect and classify the genes.

Apart from the temporal order of gene expression, phosphoproteomic responses of key signalling molecules in mouse liver occur within ~ 10 min (44) . Some genes such as *G6pase* responds rapidly (< 60 min) (8). Some metabolic enzymes and metabolites show slow dynamics (through 480 min) (9, 10). Taken together with our results of the difference of the IRG expressions, if we consider all the IRGs selected in this study as the late response genes, the putative scenario of IRG expressions and

metabolic regulation in liver can be highlighted in Fig. 19. Metabolic responses may be clustered depending on the response speeds of corresponding metabolic enzymes and genes.

In conclusion, we found that the temporal patterns and doses of insulin selectively control expression of up-regulated and down-regulated IRGs. In the future, analysis of the upstream of IRGs, including insulin signaling and transcription, is needed to address the mechanism of how temporal patterns and doses of insulin are encoded into the expression patterns of the up-regulated and down-regulated IRGs. Especially In particular, it is important to integrate the analyses of transcription, transcription factor activity (from ChIP experiments, for example), and RNA splicing because the speed of transcriptional responses depends on binding affinity, number, combination of transcription factors, and on efficiency of intron removal (12, 35). In addition, the downstream functions of the IRGs are necessary to fully address how temporal patterns and doses of insulin selectively regulate multiple biological functions. Understanding these processes will enable us to develop a new strategies to treat obesity and type 2 diabetes associated with aberrant insulin production or tissue responsiveness.

5. Figures and Figure Legends

Figure 1

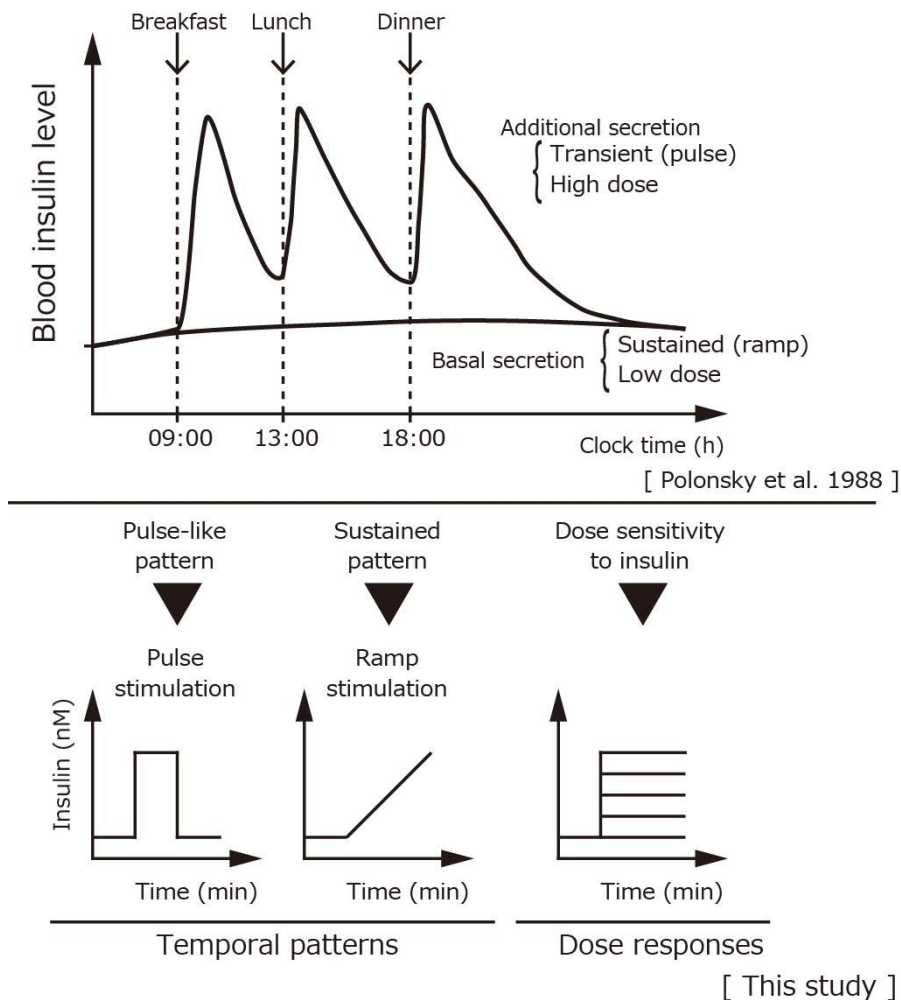


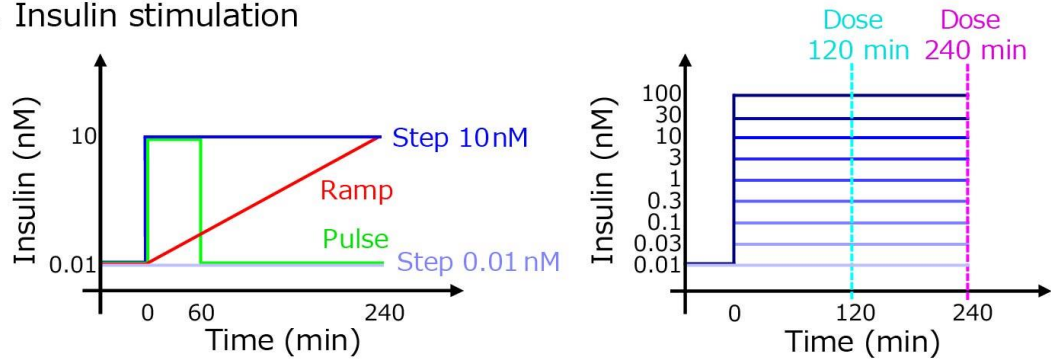
Figure 1. Experimental design of insulin stimulation patterns based on *in vivo* temporal patterns of blood insulin.

The additional insulin secretion is characterized by the pulse-like transient increase with a high dose (approximately on the order of nM with a duration of approximately 3 h), and the basal secretion is characterized by the ramp-like sustained increase with a low dose (approximately on the order of tens pM with a duration of approximately 10 h [overnight fasting]) (4). Based on *in vivo* temporal patterns of insulin, I designed the pulse stimulation and high doses of insulin and the ramp

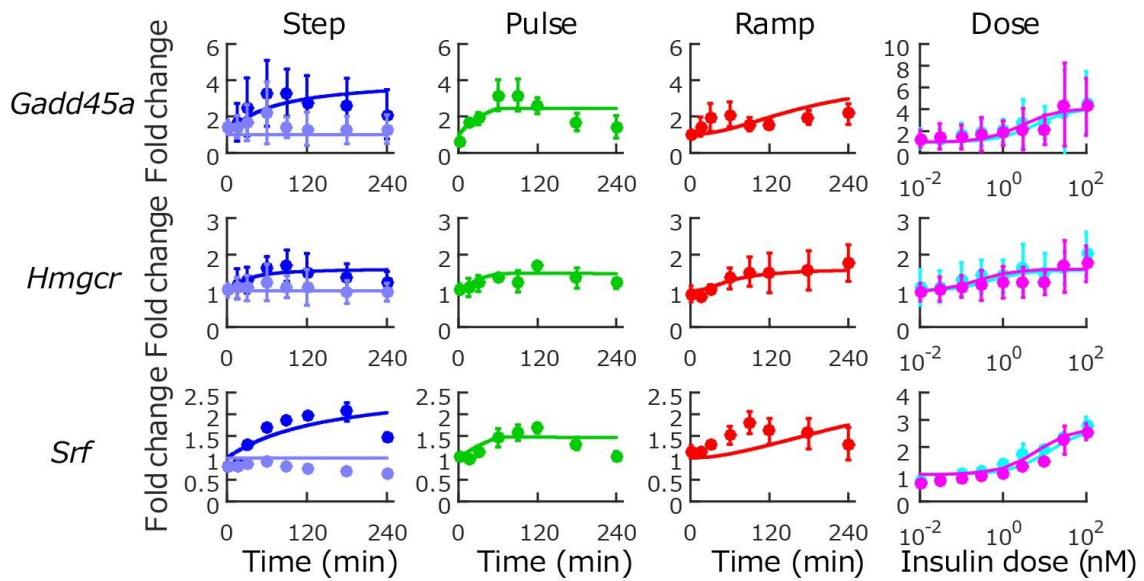
stimulation and low doses, which resemble additional and basal secretion of insulin, respectively.

Figure 2

A. Insulin stimulation



B. Up-regulated IRGs



C. Down-regulated IRGs

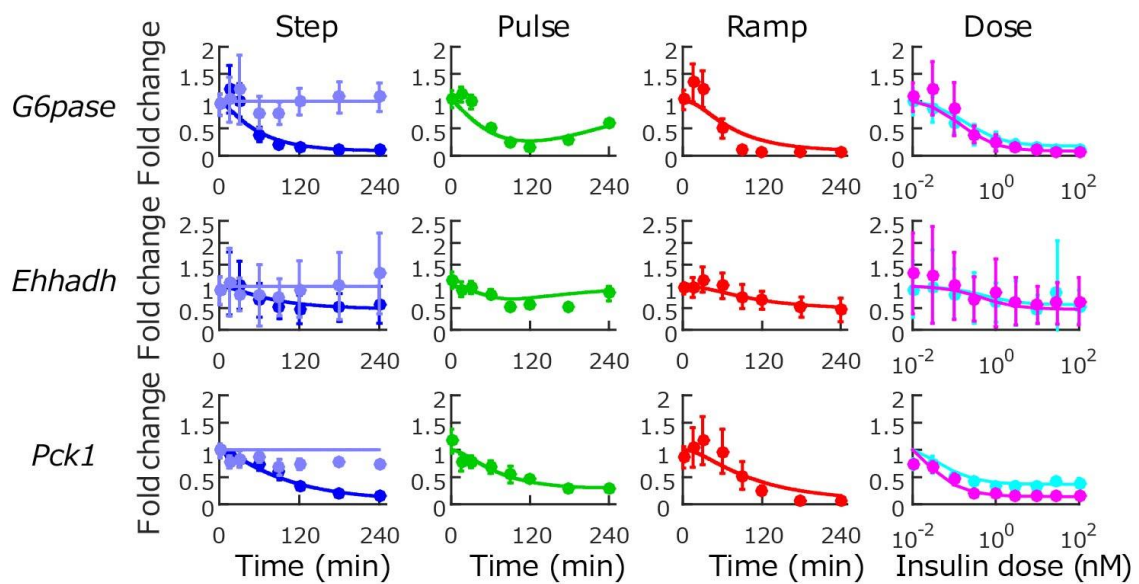


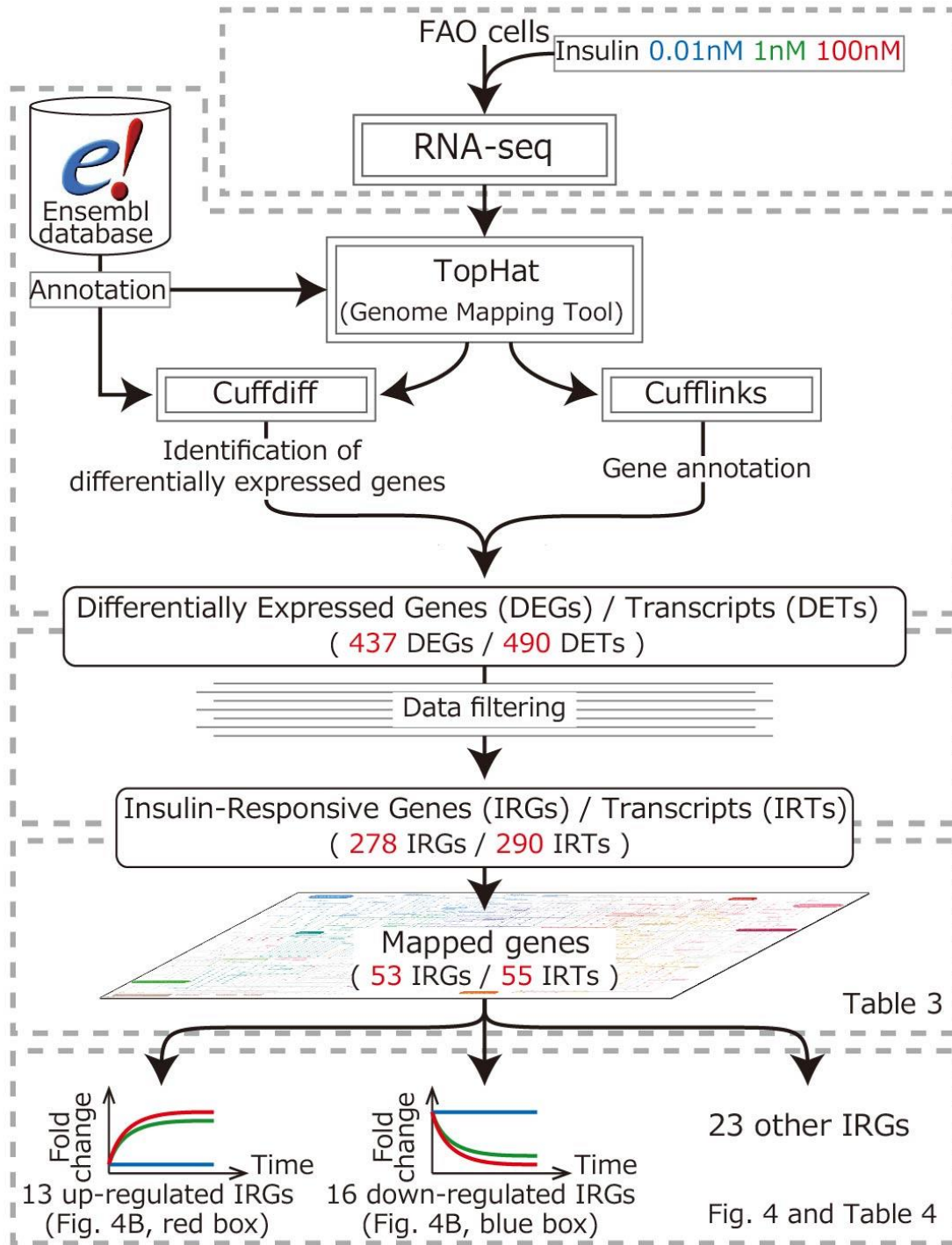
Figure 2. Responses of the IRGs to step, pulse, and ramp stimulations and to different doses of

insulin.

(A) Insulin stimulation conditions. Left: Step stimulations to 0.01 or 10 nM insulin and the pulse and ramp stimulations to 10 nM insulin. Insulin concentration by ramp stimulation increases linearly. Right: Step stimulations used to obtain the dose-response data at 120 and 240 min. (B) Responses of selected up-regulated and down-regulated IRGs to the different insulin stimulation conditions and results of simulations. The insulin stimulation conditions are listed above the graphs. Dots are experimental data of means \pm SD from three independent experiments, and solid lines are simulation data of the mathematical models (Fig. 12). Dark blue, green, and red circles and lines correspond to the responses to the step, pulse, and ramp stimulations of 10 nM insulin, respectively. Light blue circles and lines correspond to the responses to step stimulation of 0.01 nM insulin. Cyan and magenta circles and lines correspond to the dose response at 120 and 240 min, respectively. All measurements and simulations are normalized by the mean values at 0 min. Responses of all the up-regulated and down-regulated IRGs are shown in Fig. 8.

Figure 3

A



B

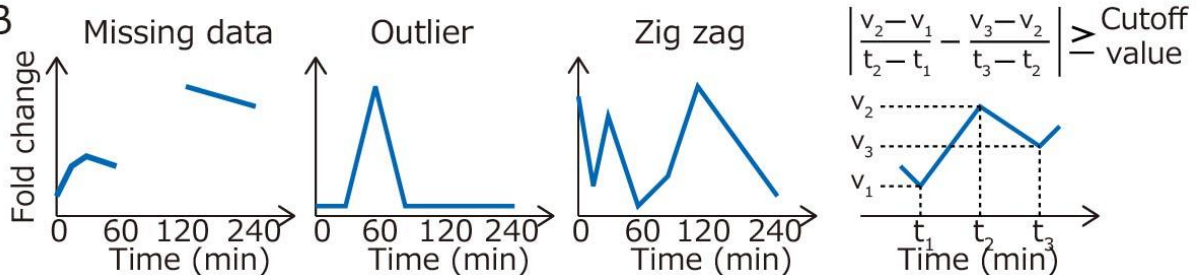
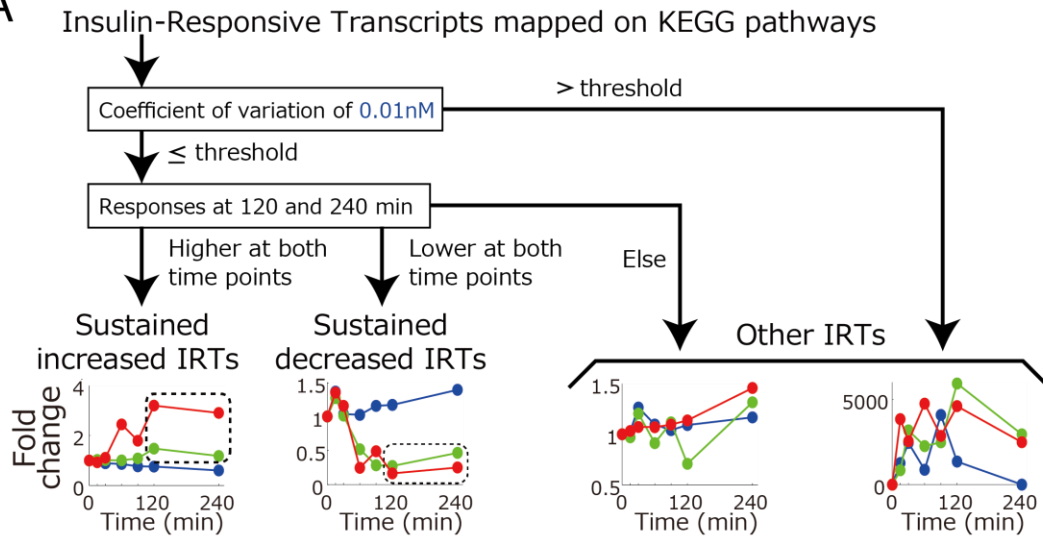


Figure 3. A pipeline for identification of the IRGs by RNA-seq.

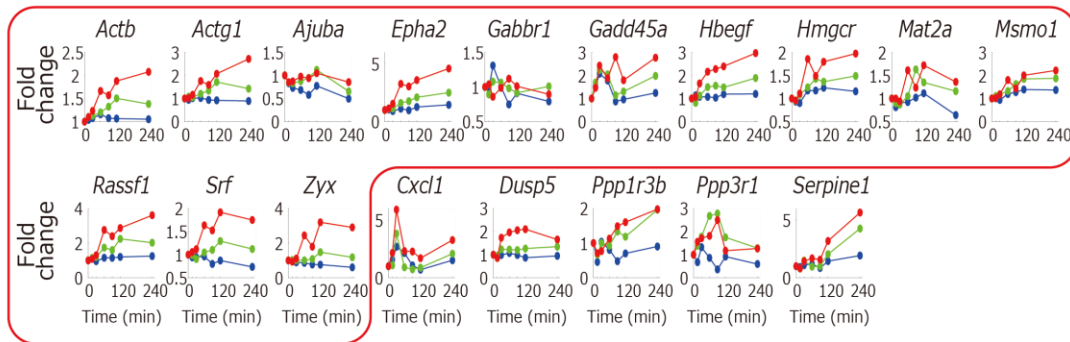
(A) The IRG identification procedures by RNA-seq that resulted in the selection of 13 up-regulated and 16 down-regulated IRGs from the 53 IRGs. Blue, green, and red solid lines describe the responses to step stimulation with 0.01, 1, and 100 nM insulin, respectively. (B) Data filtering of the differentially expressed transcripts for identification of IRTs. Differentially expressed transcripts with missing points, outliers, or zigzag patterns were excluded. The definition of zigzag patterns is shown as the last graph.

Figure 4

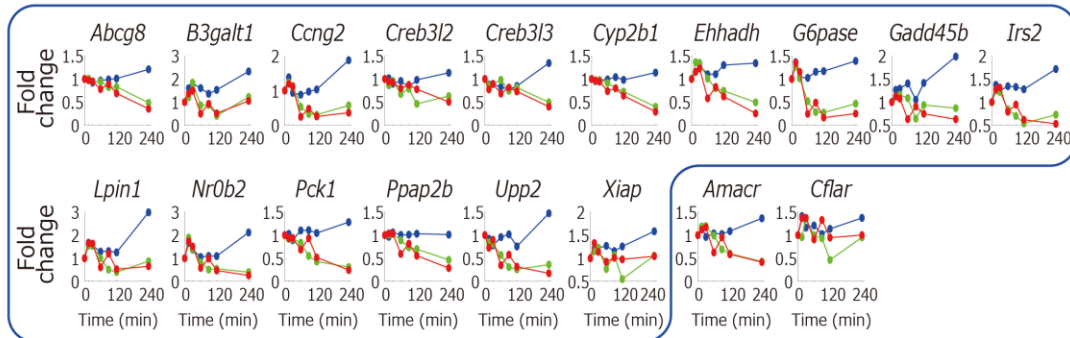
A



B Sustained increased IRTs



Sustained decreased IRTs



Other IRTs

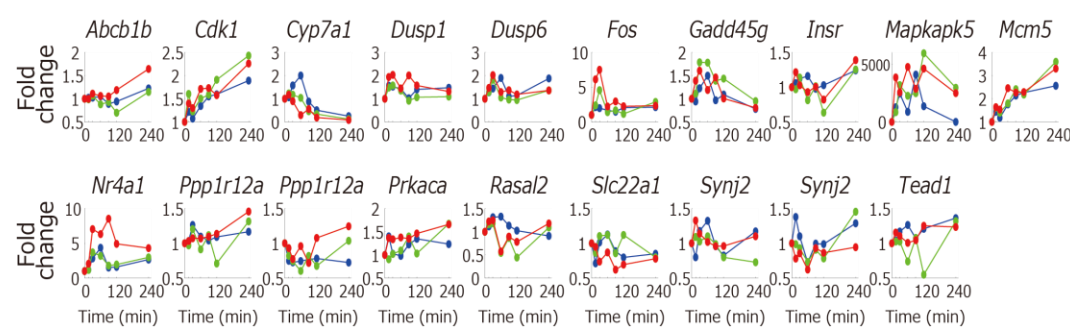
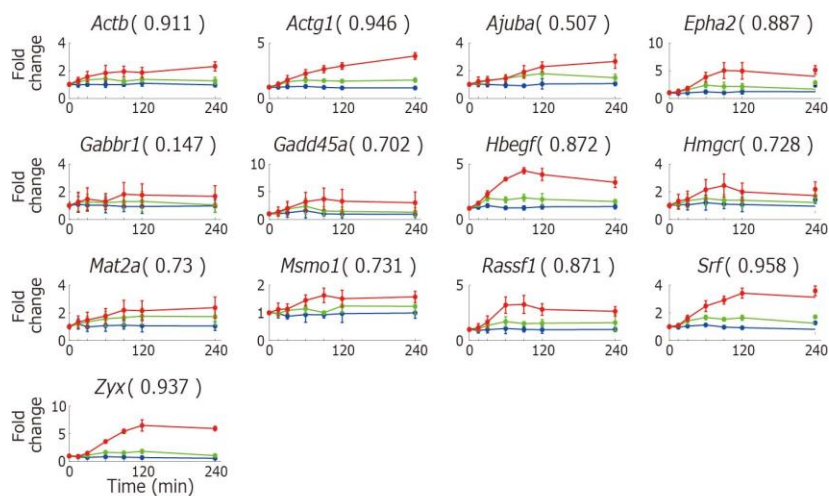


Figure 4. Selection of the up-regulated and down-regulated IRGs.

(A) The 55 IRTs corresponding to the 53 IRGs were classified into sustained increased IRTs, sustained decreased IRTs, and the other IRTs. Blue, 0.01 nM insulin; green, 1 nM insulin; red, 100 nM insulin. (B) Expression patterns of the sustained increased, sustained decreased, and the other IRTs. The names of the IRGs are substituted for those of the IRTs. The IRGs in the red and blue boxes indicate the up-regulated and down-regulated IRGs, respectively.

Figure 5

A Up-regulated IRGs



Down-regulated IRGs

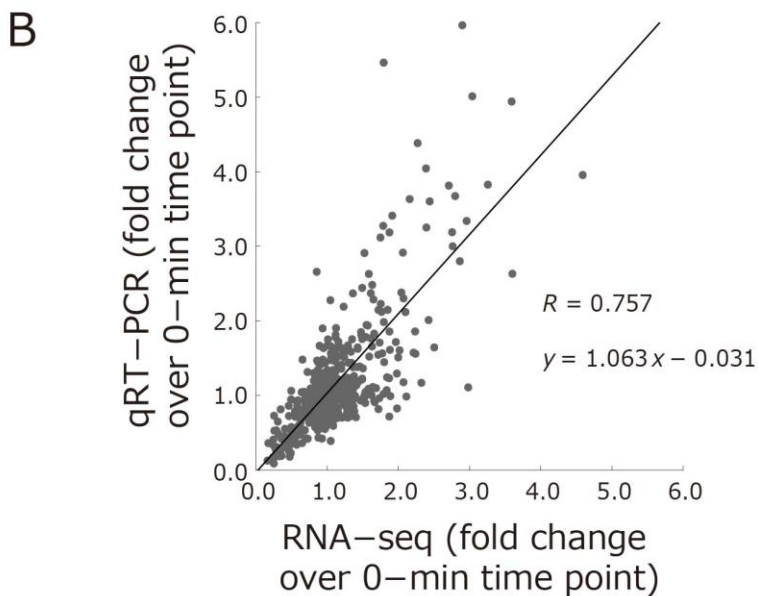
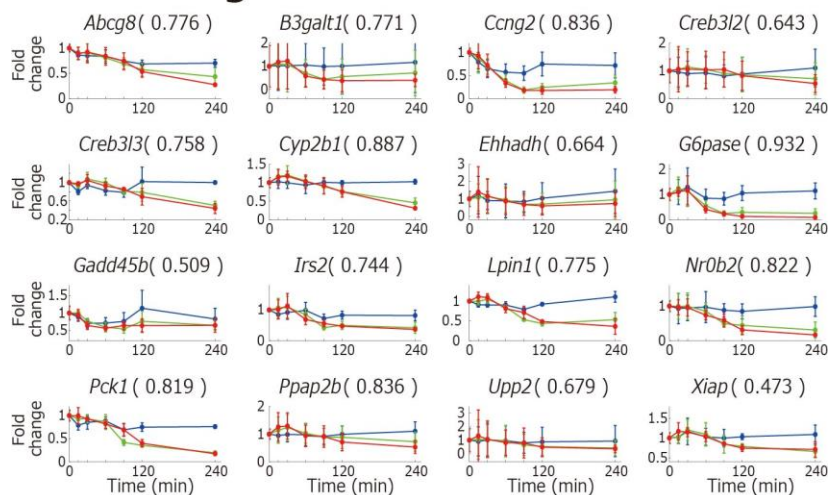


Figure 5. The expression amounts of the up-regulated and down-regulated IRGs measured by RNA-seq and qRT-PCR.

(A) The expression patterns of the up-regulated IRGs and down-regulated IRGs were measured by quantitative RT-PCR (qRT-PCR) experiments. Data are shown as means \pm standard deviations from three independent experiments. Blue, 0.01 nM insulin; green, 1 nM insulin; red, 100 nM insulin. The Pearson's correlation coefficients between RNA-seq and qRT-PCR measurements are in parentheses.

(B) Correlations of the expression amounts of the up-regulated and down-regulated IRGs between by RNA-seq and qRT-PCR measurements. Each dot represents the expression amounts of the up-regulated and down-regulated IRGs at the same time point. A Pearson's correlation coefficient (R) and a regression equation are indicated.

Figure 6

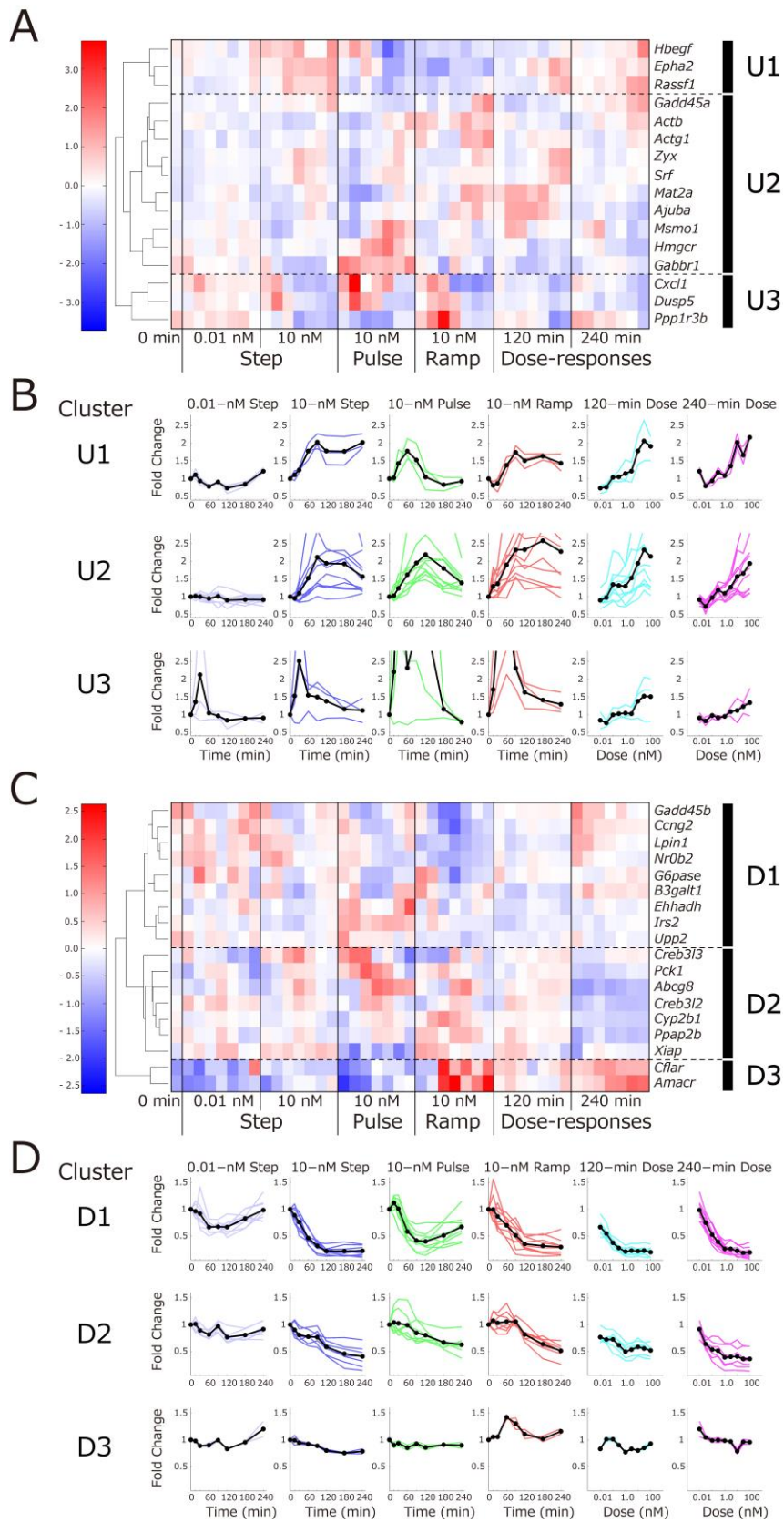


Figure 6. Hierarchical clustering of expression patterns of up-regulated and down-regulated IRGs.

(A) A dendrogram by hierarchical clustering of the expression patterns of the 16 sustained increased IRGs. Each row in the heatmap contains normalized data from each IRG in response to control media (0 min), the step stimulation (15, 30, 60, 90, 120, 180, and 240 min, from left to right column), the pulse stimulation (15, 30, 60, 90, 120, 180, and 240 min, from left to right column), the ramp stimulation (15, 30, 60, 90, 120, 180, and 240 min, left to right column), and the dose-responses (0.03, 0.1, 0.3, 1.0, 3.0, 30, and 100 nM insulin) at 120 and 240 min. Thirteen sustained increased IRGs in clusters U1 and U2 were selected as the up-regulated IRGs. The sustained increased IRGs in cluster U3 responded to the media change with the basal conditions (0.01 nM insulin) and were excluded from further study. The color bar represents the normalized expression amounts (see Materials and Methods). (B) The expression patterns of the sustained increased IRGs. Thin and thick lines indicate the expression pattern of each IRG in the indicated cluster and its mean, respectively. (C) A dendrogram by hierarchical clustering of the expression patterns of the 18 sustained decreased IRGs. Sixteen sustained decreased IRGs in clusters D1 and D2 were selected as the down-regulated IRGs. Because the responses of the sustained decreased IRGs in cluster D3 were weak, they were excluded. (D) The expression patterns of the sustained decreased IRGs. The heatmaps in (A) and (C) show normalized expression amounts, while those for time course in (B) and (D) do not because of easier understanding of the features. For clustering analysis, I used technical triplicates of a single

biological replicate as an initial screening. For the analysis of the up-regulated and down-regulated

IRGs in Fig. 11, I used biological triplicates.

Figure 7

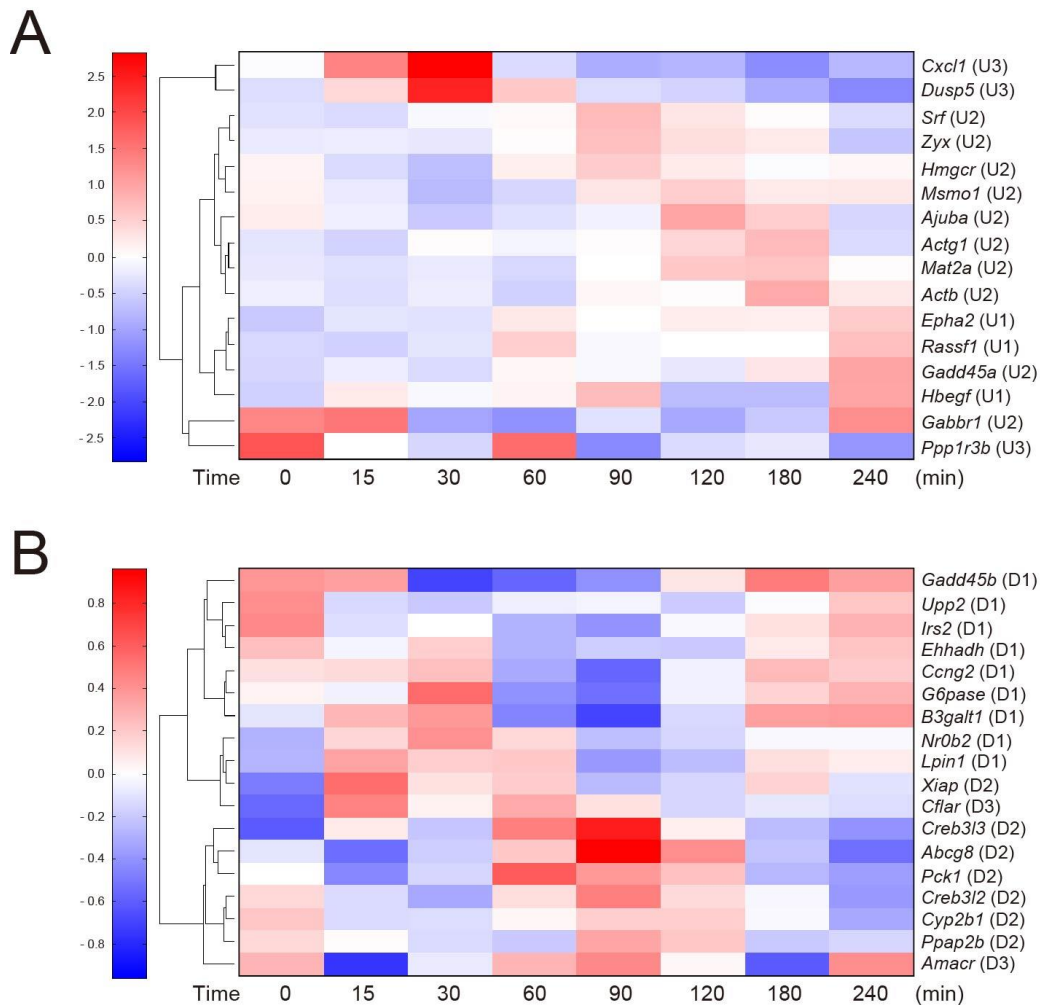
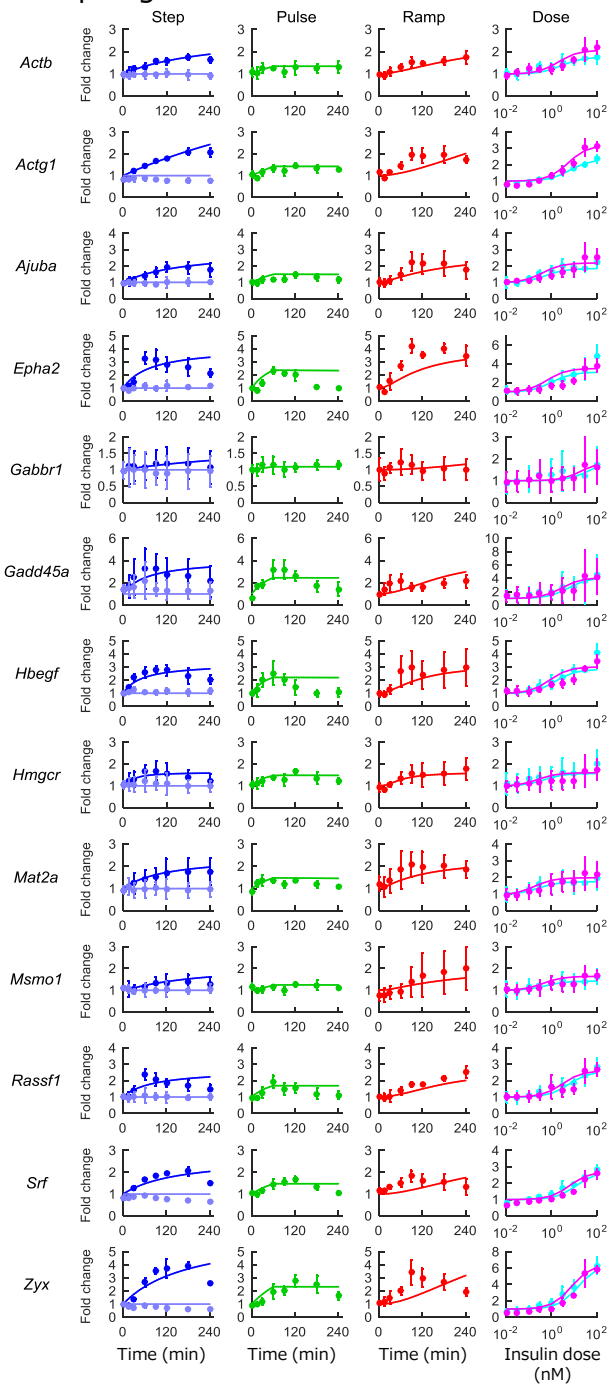


Figure 7. Hierarchical clustering by the step stimulation alone.

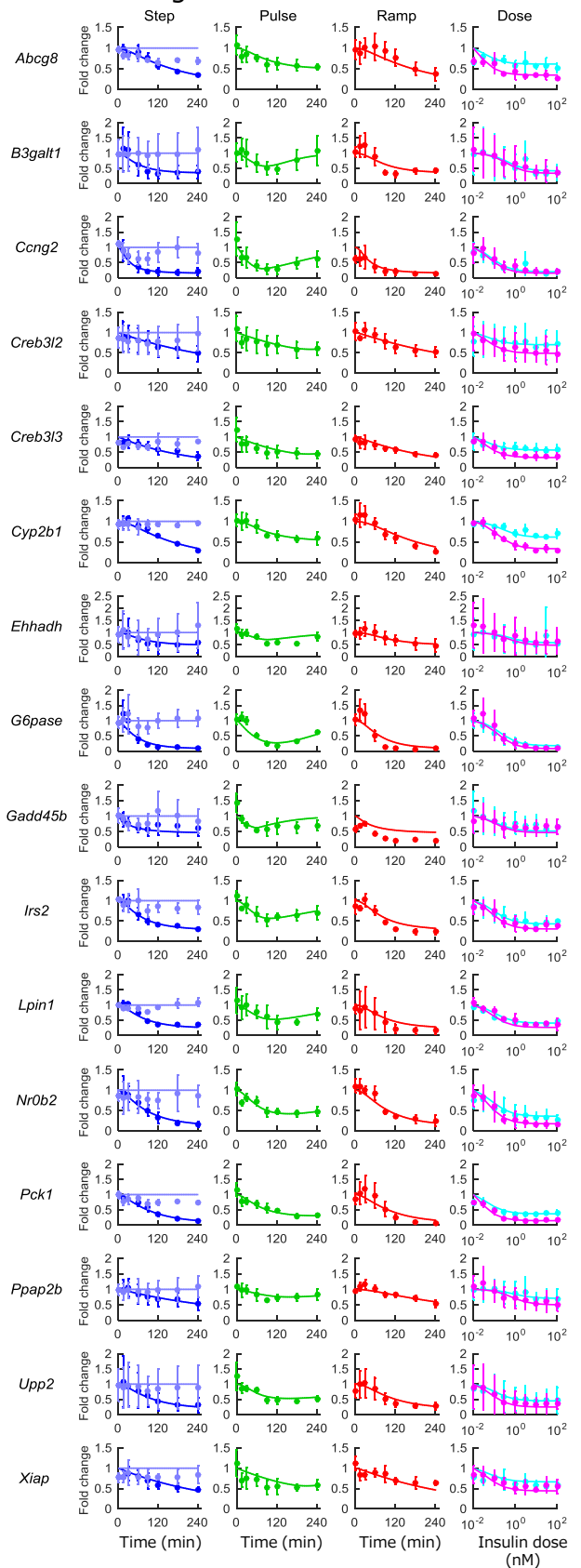
Hierarchical clustering using qRT-PCR data of the sustained increased or decreased IRGs in response to a single dose (10 nM) of the step stimulation. **(A)** the sustained increased IRGs labeled with their gene symbols and cluster names U1-U3 in parentheses (see Fig. 6A). **(B)** the sustained decreased IRGs labeled with their gene symbols and cluster names D1-D3 in parentheses (see Fig. 6C). Color bar represents the normalized expression (see Materials and Methods).

Figure 8

A Up-regulated IRGs



B Down-regulated IRGs



C. Insulin stimulation

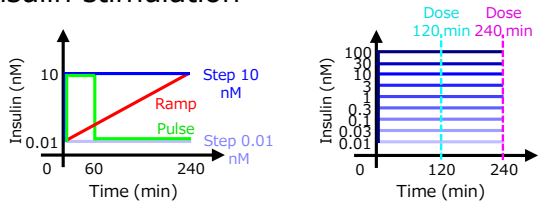
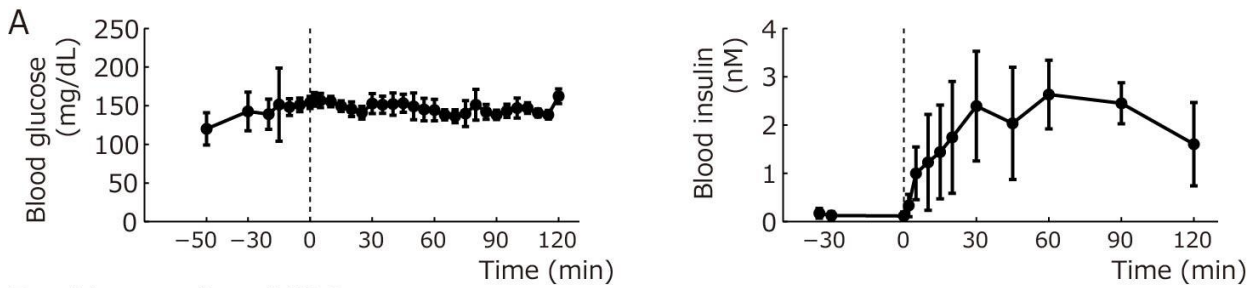


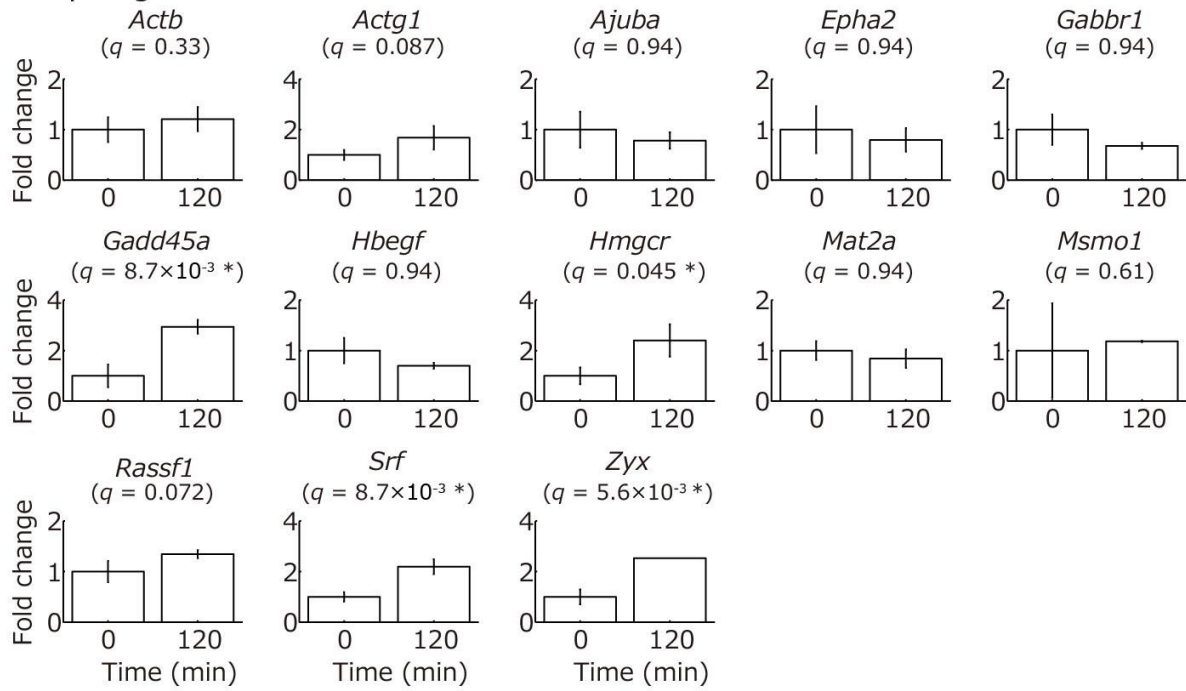
Figure 8. Responses of the IRGs to step, pulse, and ramp stimulations and the dose-responses in experiments and in simulation.

(A) Up-regulated IRGs. (B) Down-regulated IRGs. The first, second, third, and fourth columns correspond to the responses to the step, pulse, ramp, and dose-responses to insulin, respectively. Dots are experimental data and solid lines are simulation data of the mathematical models (Fig. 11). Dark blue, green, and red circles and lines correspond to the responses to the step, pulse, and ramp stimulation of 10 nM insulin, respectively. Light blue circles and lines correspond to the responses to step stimulation of 0.01 nM insulin. Cyan and magenta circles and lines correspond to the dose-response at 120 and 240 min, respectively. Error bars are the standard deviation of the mean ($n = 3$) values within independent experiments. All measurements and simulations are normalized by the mean values at 0 min. (C) Insulin stimulations. The left graph shows the step stimulations of 10 or 0.01 nM insulin and the pulse and ramp stimulations of 10 nM insulin. Insulin concentration by ramp stimulation increases linearly. The right graph shows the step stimulations used to obtain dose-responses at 120 and 240 min.

Figure 9



B Up-regulated IRGs



Down-regulated IRGs

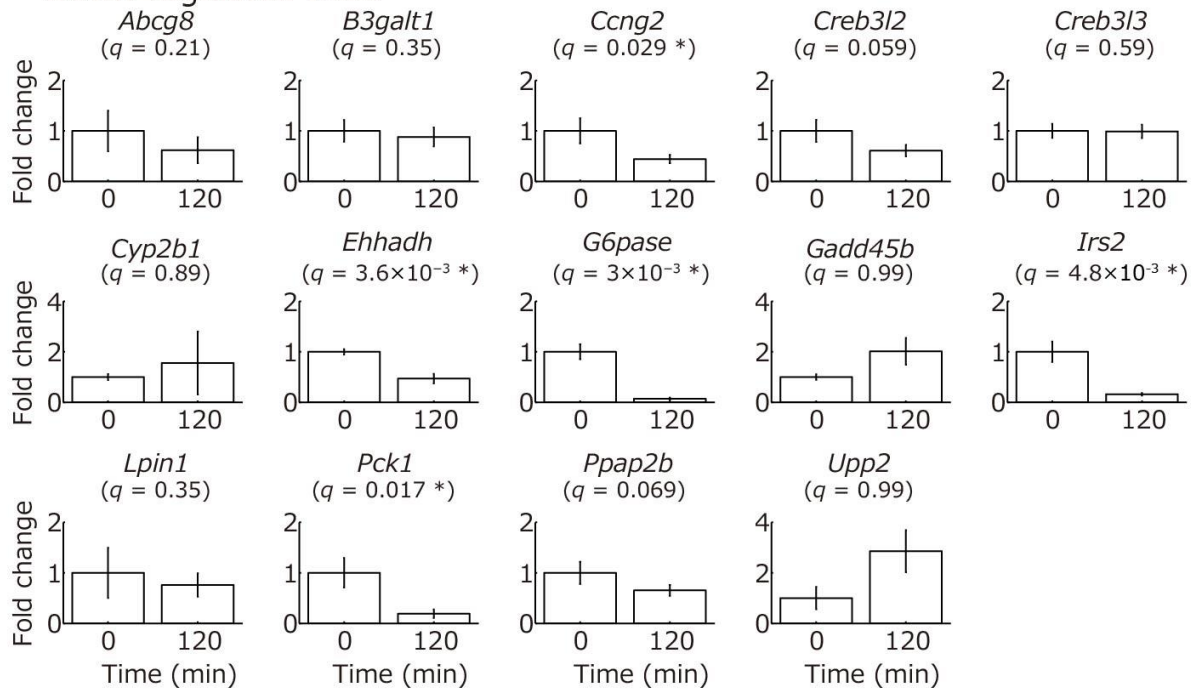


Figure 9. *In vivo* expression of the up-regulated IRGs and down-regulated IRGs in the rat liver.

(A) The concentration of blood glucose and insulin with time 0 representing the start of insulin injection. (B) The expression of the up-regulated and down-regulated IRGs in the liver. The expression of each IRG at 120 min was statistically compared with that at 0 min based on one-tailed *t* test with Benjamini-Hochberg multiple testing correction, and the adjusted *P* values are shown as *q* values. For these *in vivo* results, I considered $*q < 0.05$ as significant. These corrections were performed independently among the 13 up-regulated and the 14 down-regulated IRGs, respectively. Error bars are the SDs of the mean ($n = 3$) values within independently performed measurements. The two down-regulated IRGs, *Nr0b2* and *Xiap*, were not detected and thus are not included.

Figure 10

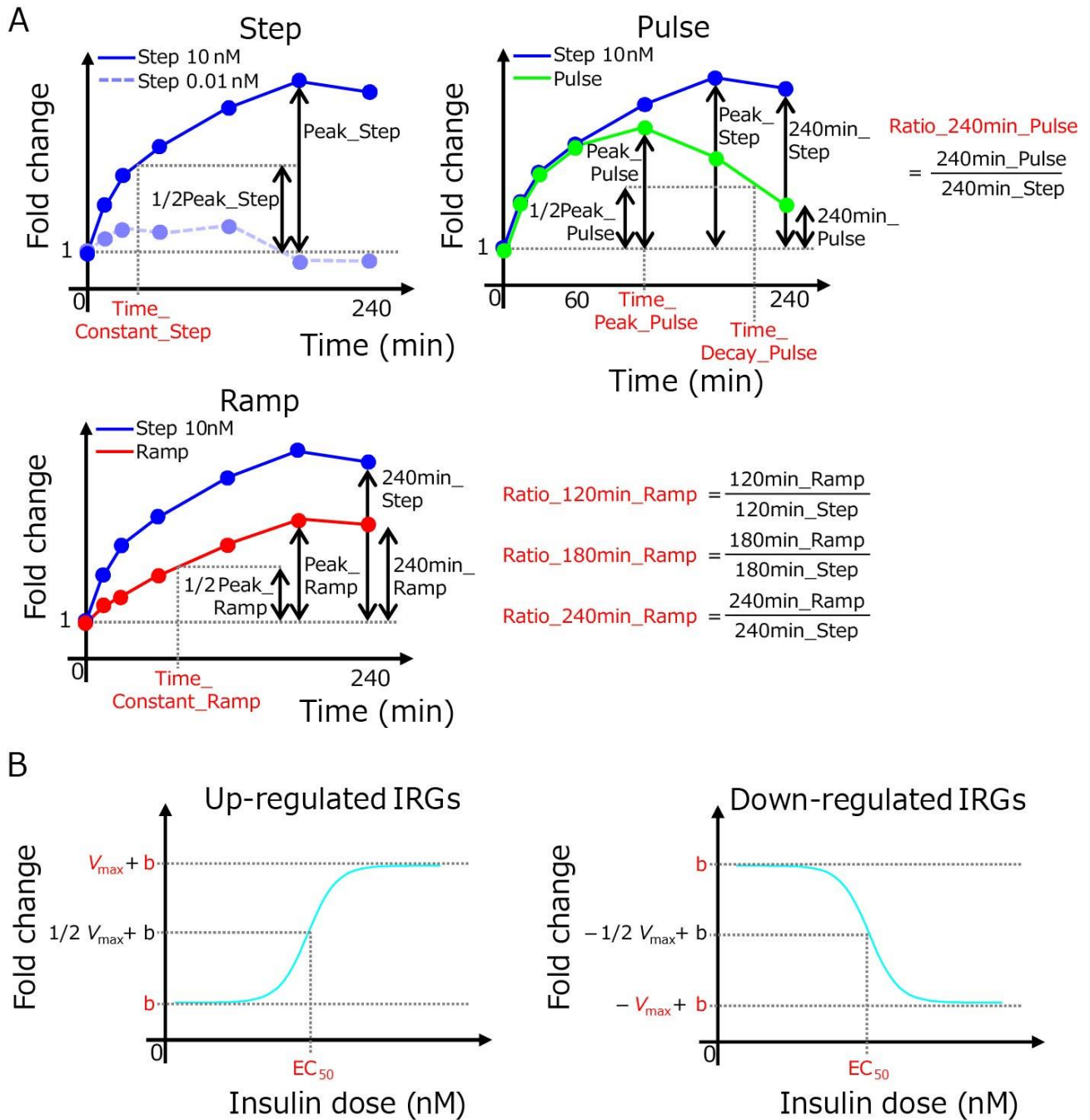


Figure 10. Defining the parameters for modeling up-regulated IRGs and down-regulated IRGs from the experimental data.

(A) Parameters of the responses of the IRGs by the step, pulse, and ramp stimulations of insulin. I calculated the parameters for the down-regulated IRGs in the same way as the up-regulated IRGs

after converting the fold change data symmetrically with respect to the line $y = 1$ (0 min). (**B**)

Parameters of the dose responses of the IRGs. The detailed definitions of the parameters can be found in Materials and Methods and Table 6.

Figure 11

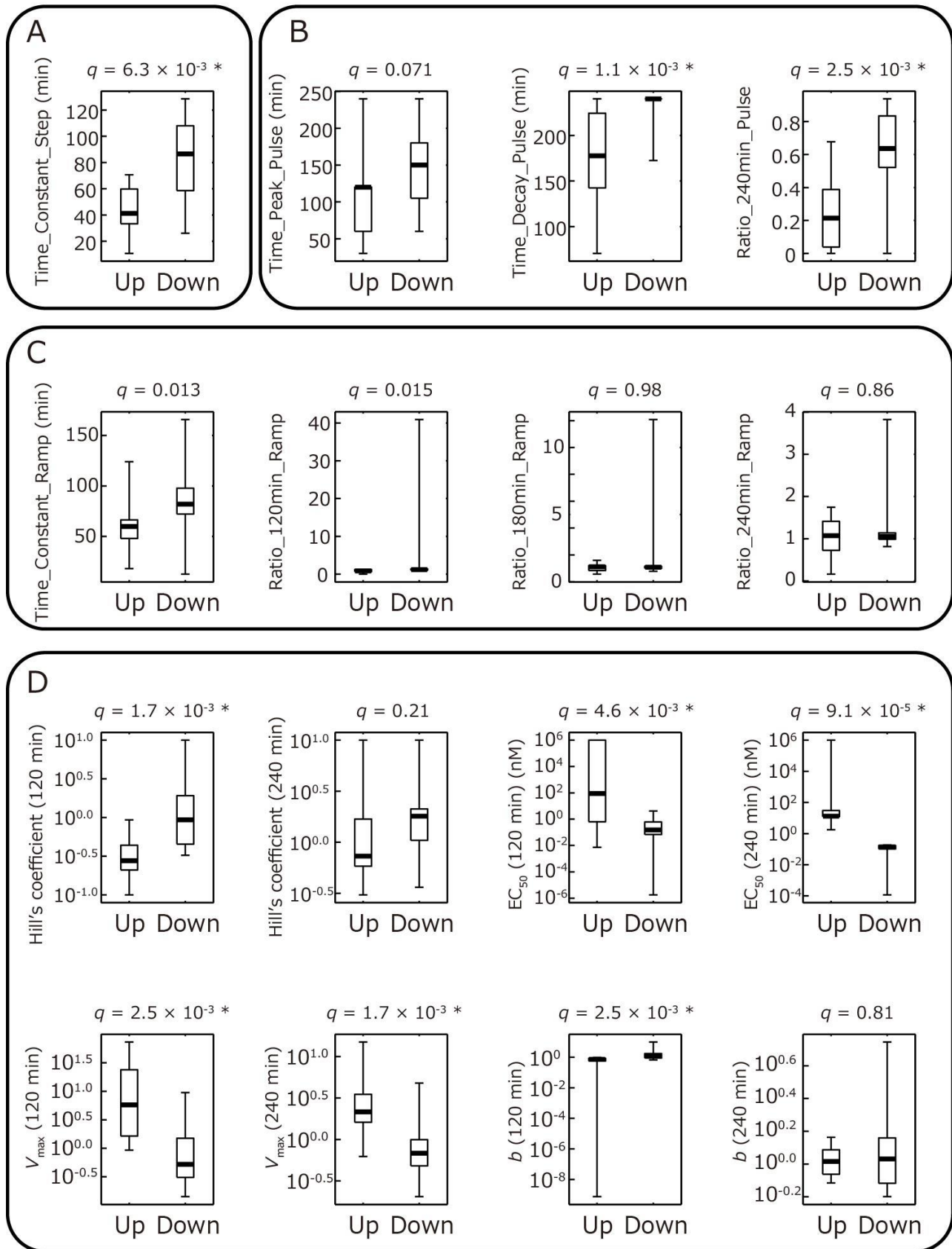
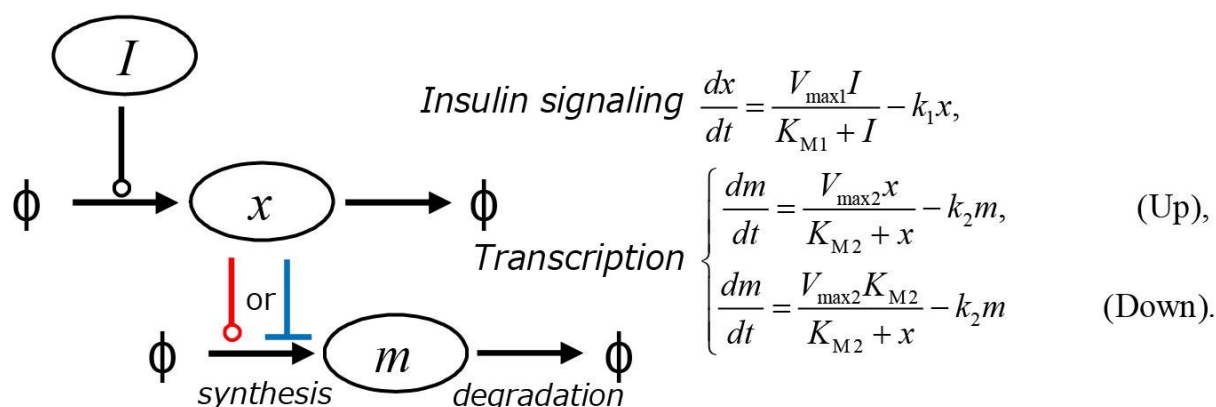


Figure 11. Comparison of the parameters for the up-regulated IRGs and down-regulated IRGs.

(A) Parameters for the step stimulation. (B) Parameters for the pulse stimulation. (C) Parameters for the ramp stimulation. (D) Parameters for the dose responses. Horizontal bold line represents the median, the box encompasses the 25th to 75th percentiles, and the whiskers indicate the maximum and minimum values. The medians of the parameters were compared between the up-regulated IRGs (Up) and down-regulated IRGs (Down) using Wilcoxon rank-sum test with the Benjamini-Hochberg multiple testing correction, and the adjusted P values are shown as q values. $q < 0.01$ were considered statistically significant ($*q < 0.01$). The values of the parameters for each IRG can be found in Table 8.

Figure 12

A



B

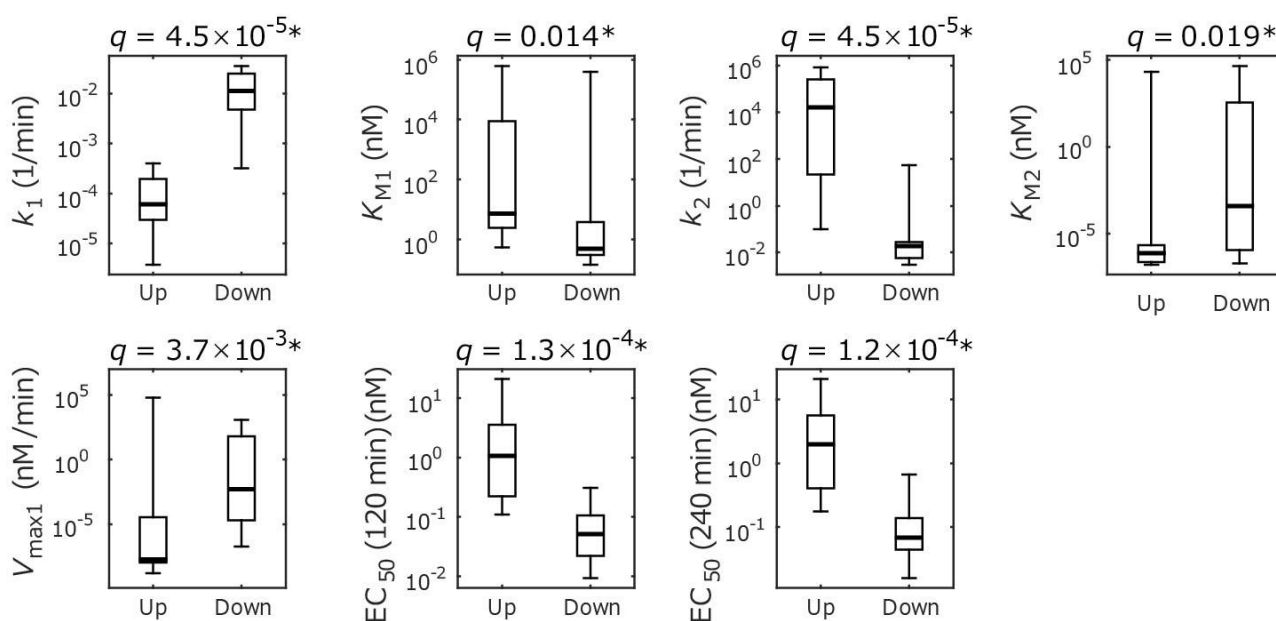


Figure 12. Mathematical models of the pathway for the up-regulated IRGs and down-regulated IRGs.

(A) The structure of the mathematical model. The model consists of two parts: (i) signaling from the insulin receptor to transcription (insulin signaling) (the upper equation) and (ii) transcription (the lower equations) (see Materials and Methods). Arrows indicate reactions, and lines with a circle or a bar indicate activation or inactivation, respectively. In the equations, I , x , and m stand for the concentrations of insulin, an insulin signalling-dependent transcriptional regulator, and the mRNAs

of the IRGs, respectively. Simulation results for all tested IRGs and stimulation conditions are shown as solid lines in Fig. 8. All parameters in each IRG model are shown in Table 9. **(B)** Box plots of the estimated parameters and the simulated EC_{50} at 120 or 240 min for the up-regulated IRGs and down-regulated IRGs. Horizontal bold line represents the median, the box encompasses the 25th to 75th percentiles, and the whiskers indicate the maximum and minimum values. The medians of the parameters were compared between the up-regulated and down-regulated IRGs using Wilcoxon rank-sum test with the Benjamini-Hochberg multiple testing correction, and the adjusted P values are shown as q values. $q < 0.01$ were considered statistically significant ($*q < 0.01$).

Figure 13

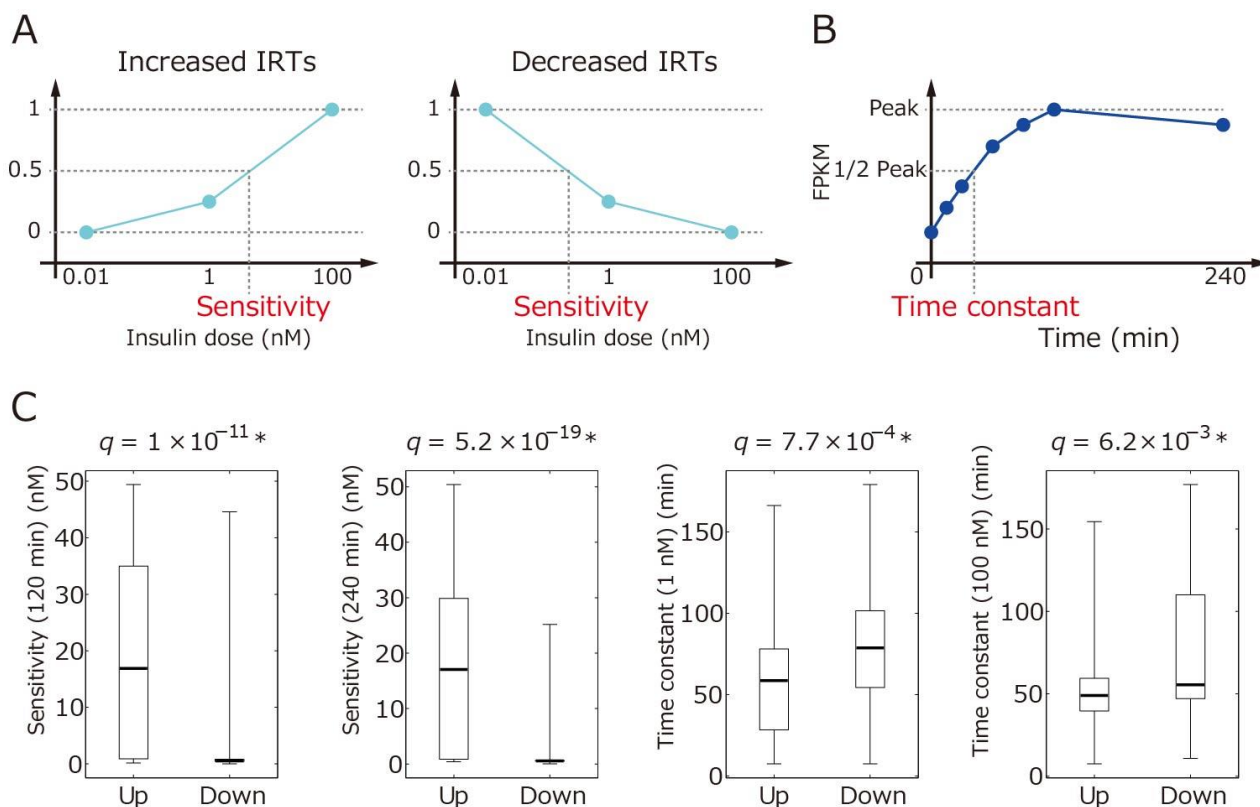
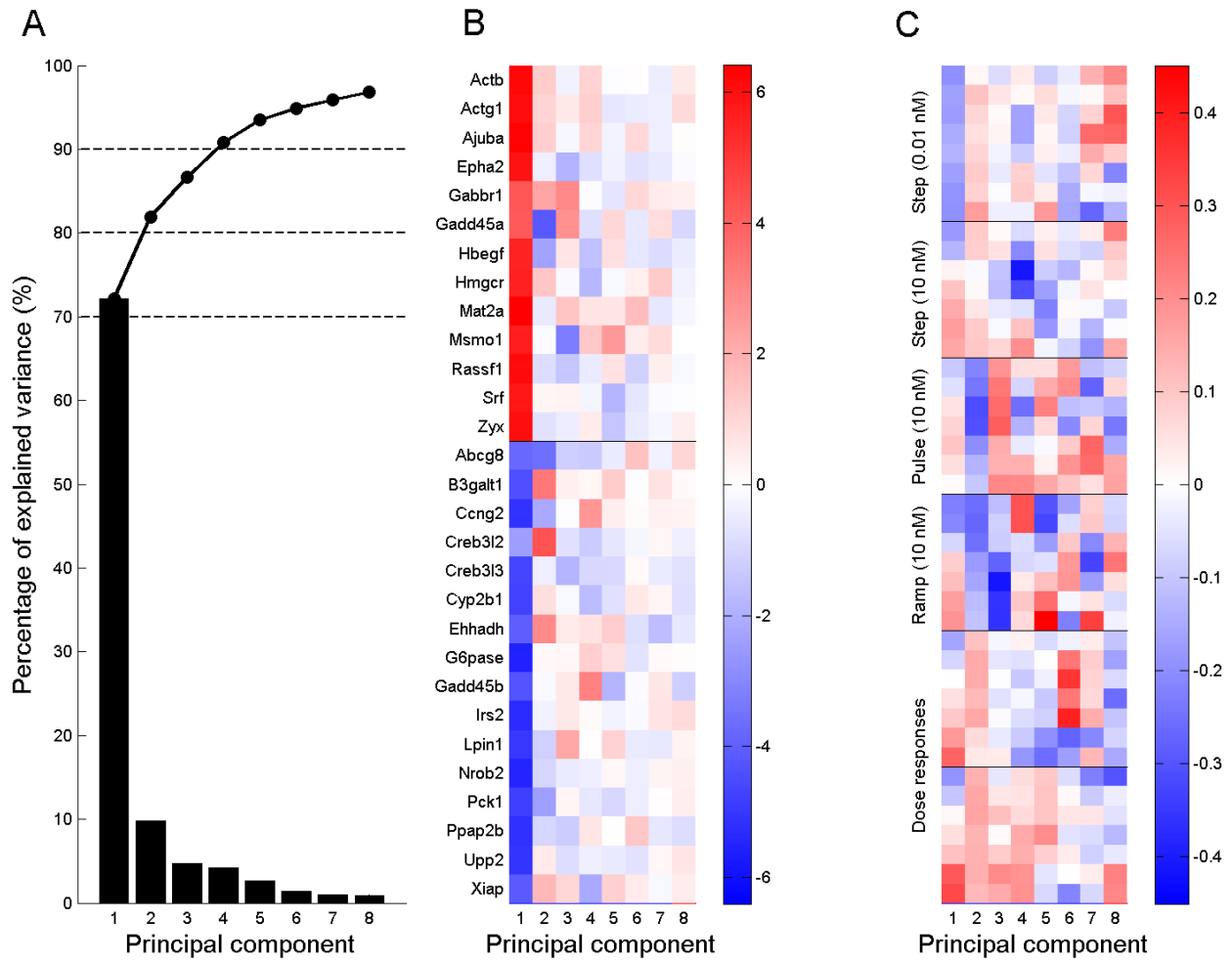


Figure 13. Sensitivity and time constants of the increased and decreased IRTs from the RNA-seq data.

Among all the 290 IRTs (Fig. 3), I identified 70 increased and 87 decreased IRTs whose FPKM values at 120 and 240 min with 1 and 100 nM insulin stimulations were higher or lower than both those of the control (0.01 nM insulin) and those of the 0 min, respectively. **(A)** Sensitivity index was defined by the insulin-dose responses which gives the 50% activation or inhibition between 0.01 nM and 100 nM insulin stimulation at 120 or 240 min. **(B)** Time constant was defined as the time when the response first reached 50% of the maximum or minimum amplitude within the time series of FPKM values of the increased or decreased IRTs, respectively. **(C)** Box plots of the parameters between the increased and decreased IRTs. The figure code and statistical analysis were the same as

in Figs. 10 and 11. The effective concentrations of insulin of the decreased IRGs at 120 min and 240 min were significantly higher than those of the increased IRGs, indicating the higher sensitivity of the decreased IRGs. The time constants of the increased IRGs by 1 nM and 100 nM of insulin were significantly faster than those of the decreased IRGs, indicating the faster response of the increased IRGs. Wilcoxon rank sum test with the Benjamini-Hochberg multiple testing correction, and the adjusted *P* values are shown as *q* values. The *q* values < 0.01 were considered statistically significant (**q* value < 0.01). Gene names and the time course data of the increased and decreased IRGs can be seen in Supplementary Materials (data file S8, which can be downloaded from <http://stke.sciencemag.org/content/9/455/ra112>).

Figure 14



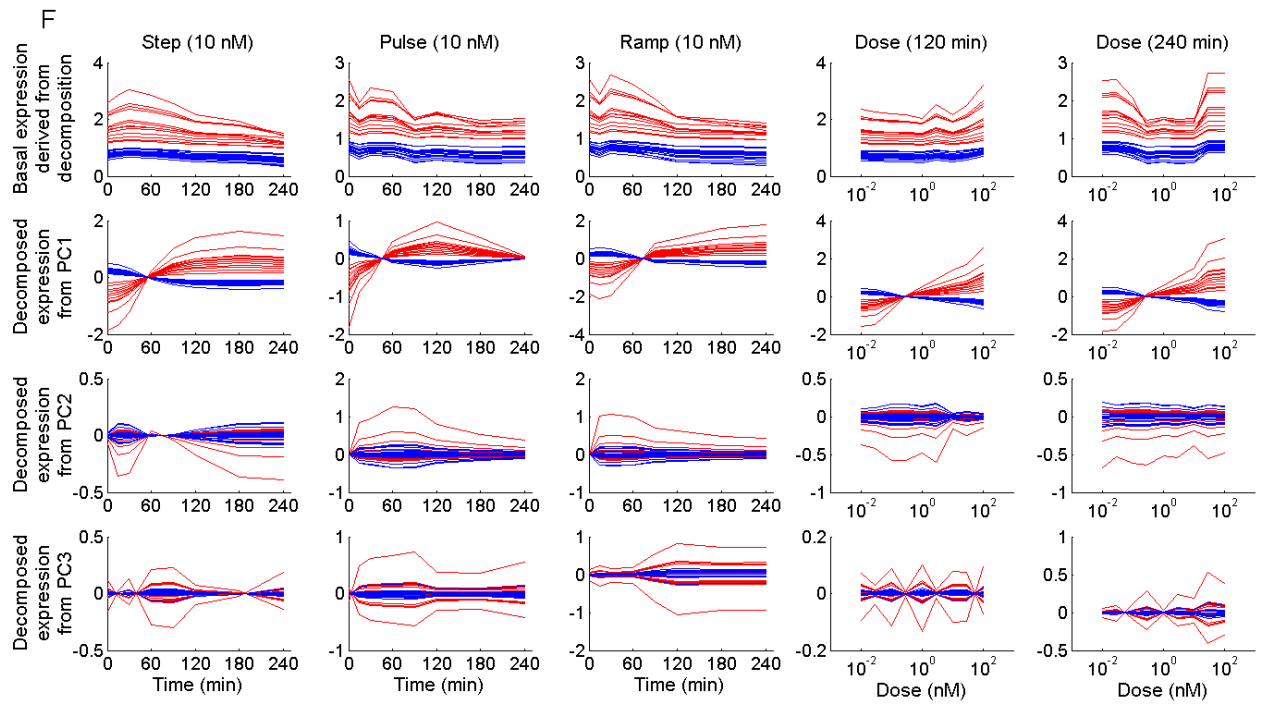
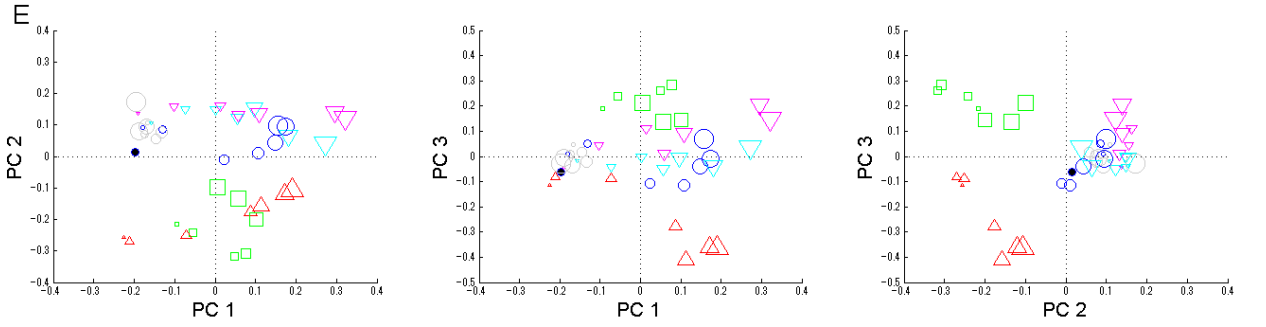
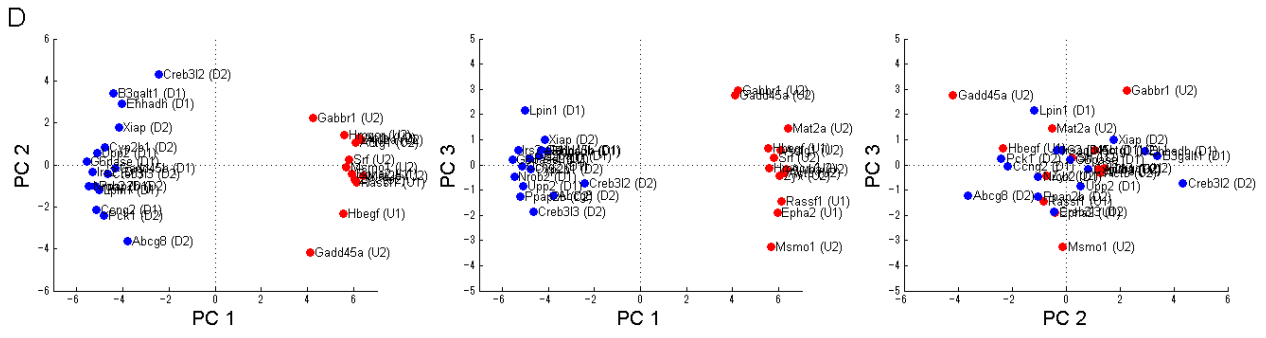


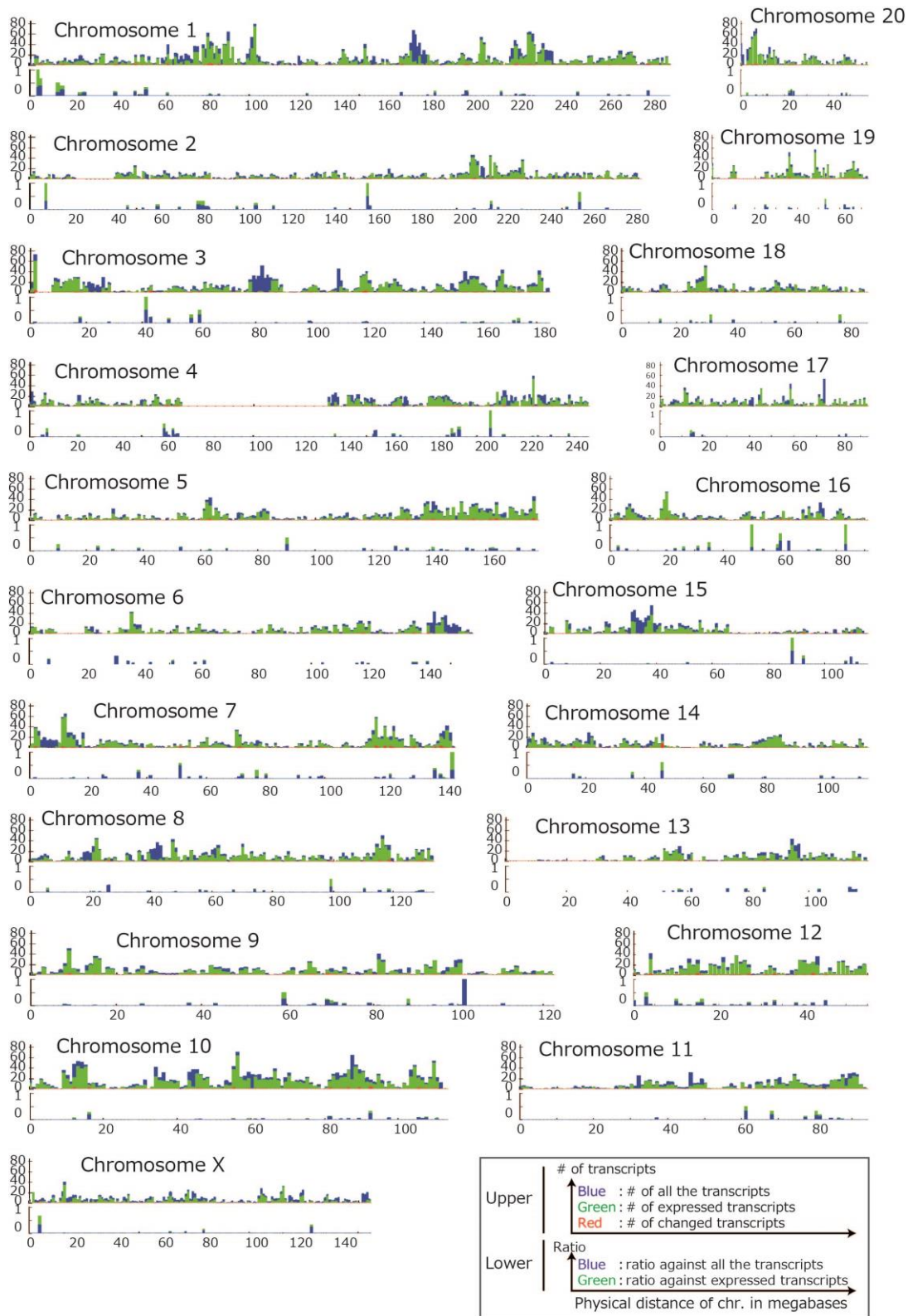
Figure 14. Analysis of response characteristics of the up-regulated and down-regulated IRGs by principal component analysis using various patterns of insulin stimulation.

(A) Percentage of explained variances. Contributions of each principal component are shown as bar plots. The cumulative contribution is shown as a line chart. Up to 3 principal components, cumulative contribution of the explained variances exceeded more than 80%. (B) Heat map of the score matrix of the up-regulated and down-regulated IRGs. Up to 8 principal components are shown. Color bar represents strength of the score. Gene names are listed in the vertical direction on left side. The 13 upper and 16 lower genes are the up-regulated and down-regulated genes, respectively. (C) Heat map of a loading matrix of all the stimulation patterns. Up to eight principal components are shown. Color bar represents strength of the loading. Gene names are listed in the vertical direction on left side. (D) Scatter plots of the score of the PC 1 to 3. Red and blue dots represent each of the up-regulated and down-regulated IRG, respectively. Up-regulated and down-regulated IRGs were separated in the PC1 direction. So far, we can not explain what the PC 2 and 3 score distinguish. (E) Scatter plots of the loading of the PC 1 to 3. A black dot, gray circles, blue circles, green squares, red triangles, cyan inverted triangles, and magenta inverted triangles represent 0-min response, step stimulation (0.01 nM), step stimulation (10 nM), pulse stimulation (10 nM), ramp stimulation (10 nM), dose response (120 min), and dose response (240 min), respectively. The larger size of the markers, the later time points (0 to 240 min). In the PC1 direction, the larger amplitude of the response, the larger PC1 loading. In the PC2 direction, step stimulation including dose responses

were separated from pulse and ramp stimulations. In the PC3 direction, ramp, step, and pulse stimulations were separated. (F) Decomposed expression profiles using singular value decomposition up to the 3 principal components (see Materials and Methods). Red and blue line charts represent each of the up-regulated and down-regulated IRGs, respectively. PC1-decomposed expression might capture the variance at later time points for the step and ramp stimulation, at 120 min for the pulse stimulation, at high doses for the dose responses. PC2-decomposed expression might capture the variance at 15, 30, or >180 min for the step stimulation, at 60 min for the pulse stimulation, at 15-30 min for the ramp stimulation. PC3-decomposed expression might capture the variance at 60 or 90 min for the step stimulation, at 60-90 min for the pulse stimulation, at >120 min for the ramp stimulation.

Figure 15

A



B

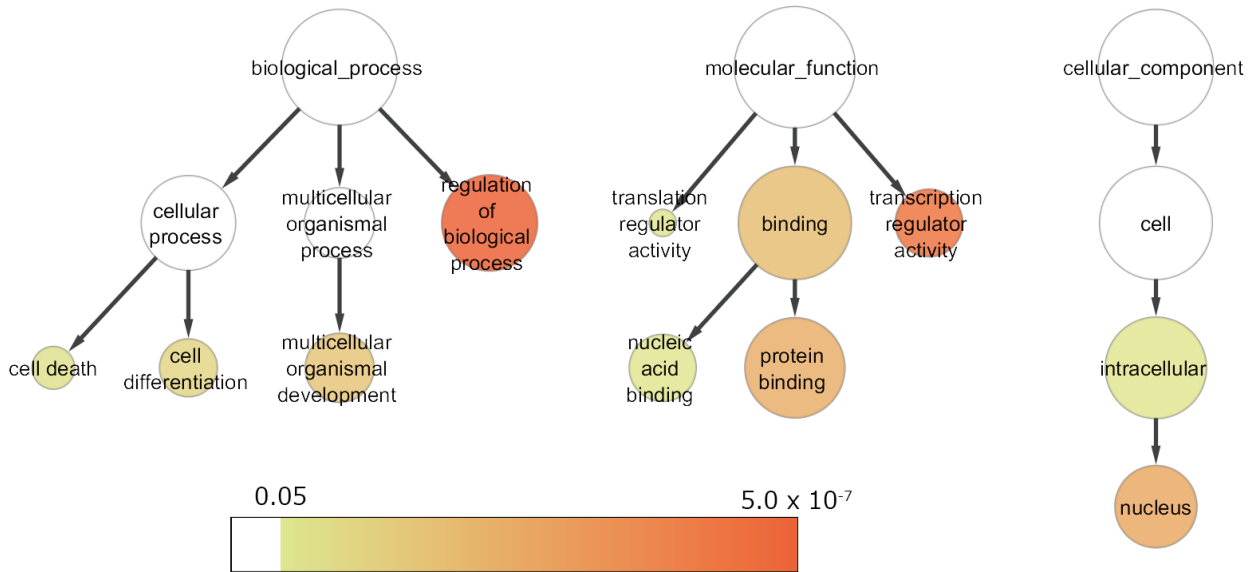


Figure 15. Chromosome mapping and gene ontology of DEGs.

(A) A chromosome map of the DEGs on the rat genome using Integrative Genomics Viewer (IGV) tool (35). Horizontal and vertical axes represent length of base pairs and number of the genes per Mbp length, respectively. Upper panels: blue, green, or red bar represents number of the transcripts registered in Ensembl database, number of the transcripts detected through Otsu method, or number of the transcripts detected as differentially expressed by Cuffdiff (FDR threshold = 0.05), respectively. Lower panels: blue or green bar represents the ratio of the transcripts detected as differentially expressed by Cuffdiff over the transcripts registered in Ensembl database or the transcripts detected through Otsu method, respectively. (B) Gene ontology analysis of the DEGs using the BiNGO tool (Cytoscape plugin BiNGO 2.44) (36). Size of a circle represents the number of the statistically over-represented genes. Color bar represents the *P* value from the hypergeometric test for over-representation with multiple testing correction using Bonferroni method (FWER) or

Benjamini-Hochberg method (FDR). I considered the corrected P value < 0.05 as statistically significant. I used GOSlim_GOA as the gene ontology.

Figure 16

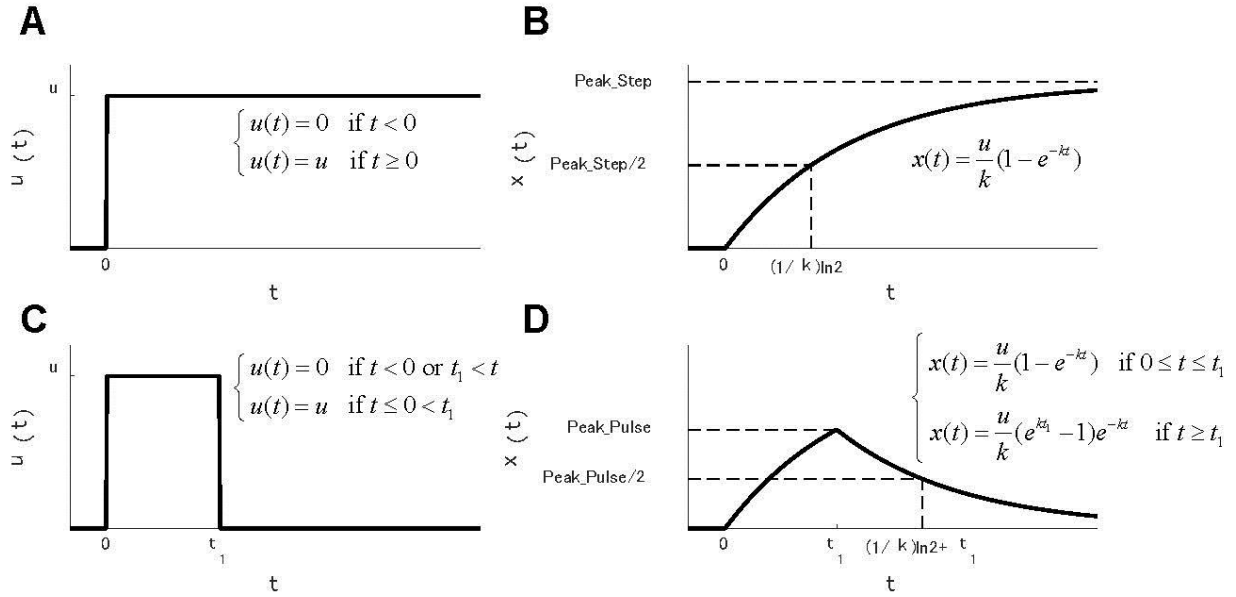


Figure 16. Decay time constant by pulse stimulation represents the time constant of a pathway.

Stimulations (u) and responses (x) of a signaling pathway approximated by first-order linear time-invariant system. **(A)** Step stimulation; **(B)** response to step stimulation; **(C)** pulse stimulation; **(D)** response to pulse stimulation. Functions of u and x are also shown.

Let a signaling pathway be approximated by the following first-order linear time-invariant system:

$$\frac{dx(t)}{dt} = u(t) - kx(t), \quad (1)$$

where $x(t)$ is an activity of a signaling molecule, $u(t)$ is an input by stimulation. k stands for the reaction constant, which is an inverse of the time constant. As for a step stimulation (Fig. 16A), $u(t)$ can be described as equation (2):

$$\begin{cases} u(t) = 0 & \text{if } t < 0, \\ u(t) = u & \text{if } t \geq 0. \end{cases} \quad (2)$$

When $x(0)$ equals zero, equation (1) for the step stimulation can be solved analytically as follows:

$$x(t) = \frac{u}{k} (1 - e^{-kt}), \quad (3)$$

where x converges u/k (Peak_Step), as t approaches infinity (Fig. 16B). When I define Time_Constant_Step as the time when $x(t)$ equals the half of Peak_Step, the time constant can be described in equation (4):

$$\text{Time_Constant_Step} = \frac{1}{k} \ln 2. \quad (4)$$

In a case for a pulse stimulation (Fig. 16C), $u(t)$ can be described as equation (5):

$$\begin{cases} u(t) = 0 & \text{if } t < 0 \text{ or } t_1 < t, \\ u(t) = u & \text{if } 0 \leq t < t_1. \end{cases} \quad (5)$$

When $x(0)$ equals zero, equation (1) for the pulse stimulation can be solved analytically as follows:

$$\begin{cases} x(t) = \frac{u}{k} (1 - e^{-kt}), & \text{if } 0 \leq t < t_1, \\ x(t) = \frac{u}{k} (e^{-kt_1} - 1) e^{-k(t-t_1)}, & \text{if } t \geq t_1, \end{cases} \quad (6)$$

where maximum x value is $(u/k)(1 - \exp(-kt_1))$ (Peak_Pulse), when t equals t_1 (Fig. 16D). When I define Time_Decay_Pulse as the time when $x(t)$ equals the half of Peak_Pulse after t_1 , the time can be described in equation (7):

$$\text{Time_Decay_Pulse} = \frac{1}{k} \ln 2 + t_1. \quad (7)$$

Using equations (4) and (7), Time_Constant_Step can be represented by Time_Decay_Pulse as Eq.

(8):

$$\text{Time_Constant_Step} = \text{Time_Decay_Pulse} - t_1. \quad (8)$$

Therefore, decay time constant, a linear function of the inverse of k , represents rapidness of the signaling pathway by both step and pulse stimulations. Although actual signaling pathways are much more complex so that strict analytical solutions are hard to be obtained, decay time constant can be regarded as an apparent time constant of the signaling pathway.

Figure 17

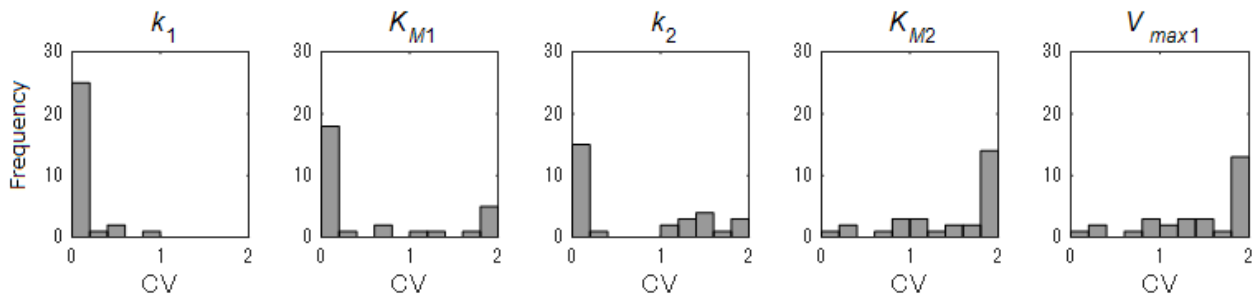


Figure 17. Histograms of coefficient of variation (CV) of parameter values in the best 5 models among the 30 models.

The coefficient of variation is quantified for each IRG in the best five models among the 30 models obtained during parameter estimation process.

Figure 18

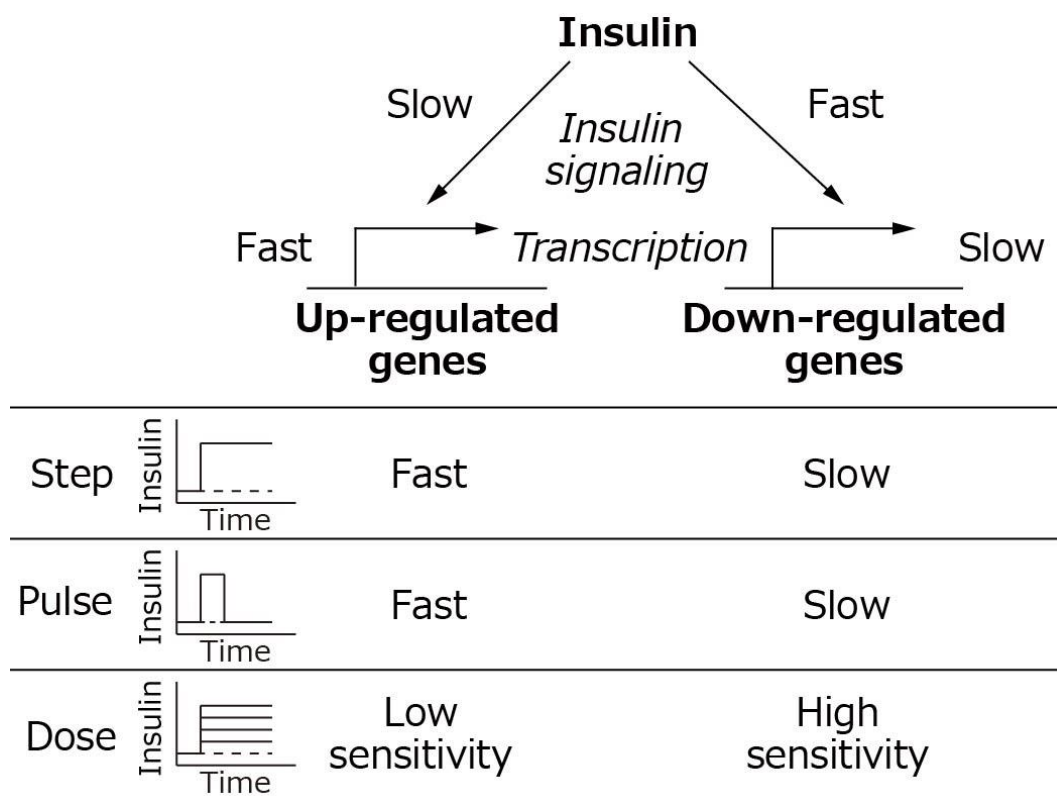


Figure 18. Selective control of the up-regulated IRGs and down-regulated IRGs by temporal patterns and doses of insulin.

Mathematical modeling revealed that insulin signaling of the down-regulated IRGs is more rapid than that of the up-regulated IRGs, whereas transcription of the up-regulated IRGs is more rapid than that of the down-regulated IRGs. In experiments, the up-regulated IRGs responded more rapidly to step and pulse insulin stimulation, whereas the down-regulated IRGs showed higher sensitivity than did the up-regulated IRGs to insulin doses.

Figure 19

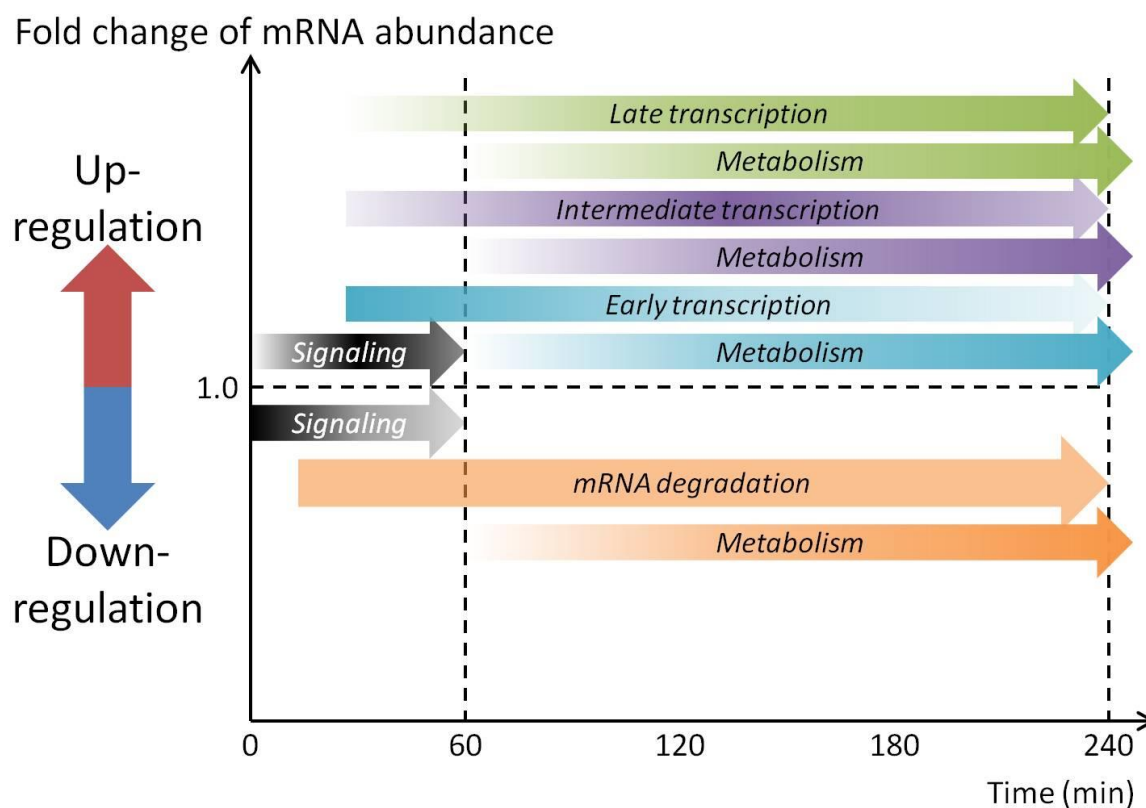


Figure 19. Putative scenario of insulin action in liver.

Previous studies (8-10, 12, 44) and our results suggest that the up-regulated and down-regulated IRGs respond to insulin stimulations at different speeds from each other. The up-regulated IRGs may be mainly regulated by slower signaling and RNA splicing, whereas the down-regulated IRGs by fast signalling and mRNA degradation. In this study, we considered only the late response genes (“Late transcription”) as the IRGs. Improvement of experimental and analytical procedures may allow us to comprehensively discuss all the groups of the gene expressions.

6. Tables

Table 1. Validation of Cuffdiff to identify the DEGs by changing the Cuffdiff's internal threshold (FDR).

	Gene symbol	FDR (sorted)	FDR threshold							
			0.001	0.005	0.01	0.05	0.1	0.5	0.9	1
Up-regulated IRGs	<i>Zyx</i>	0.0×10 ⁰	DEG	DEG	DEG	DEG	DEG	DEG	DEG	DEG
	<i>Gadd45a</i>	1.3×10 ⁻¹²	DEG	DEG	DEG	DEG	DEG	DEG	DEG	DEG
	<i>Epha2</i>	1.0×10 ⁻¹⁰	DEG	DEG	DEG	DEG	DEG	DEG	DEG	DEG
	<i>Actg1</i>	6.6×10 ⁻⁶	DEG	DEG	DEG	DEG	DEG	DEG	DEG	DEG
	<i>Srf</i>	1.3×10 ⁻⁴	DEG	DEG	DEG	DEG	DEG	DEG	DEG	DEG
	<i>Rassf1</i>	2.7×10 ⁻⁴	DEG	DEG	DEG	DEG	DEG	DEG	DEG	DEG
	<i>Ajuba</i>	0.006			DEG	DEG	DEG	DEG	DEG	DEG
	<i>Mat2a</i>	0.006			DEG	DEG	DEG	DEG	DEG	DEG
	<i>Msmo1</i>	0.007			DEG	DEG	DEG	DEG	DEG	DEG
	<i>Actb</i>	0.015				DEG	DEG	DEG	DEG	DEG
	<i>Hbegf</i>	0.025				DEG	DEG	DEG	DEG	DEG
	<i>Gabbr1</i>	0.031				DEG	DEG	DEG	DEG	DEG
	<i>Hmgcr</i>	0.046				DEG	DEG	DEG	DEG	DEG
Down-regulated IRGs	<i>Pck1</i>	1.2×10 ⁻¹²	DEG	DEG	DEG	DEG	DEG	DEG	DEG	DEG
	<i>Irs2</i>	2.7×10 ⁻⁹	DEG	DEG	DEG	DEG	DEG	DEG	DEG	DEG
	<i>Ccng2</i>	3.6×10 ⁻⁹	DEG	DEG	DEG	DEG	DEG	DEG	DEG	DEG
	<i>Lpin1</i>	2.1×10 ⁻⁶	DEG	DEG	DEG	DEG	DEG	DEG	DEG	DEG
	<i>Nr0b2</i>	3.0×10 ⁻⁶	DEG	DEG	DEG	DEG	DEG	DEG	DEG	DEG
	<i>G6pase</i>	8.3×10 ⁻⁵	DEG	DEG	DEG	DEG	DEG	DEG	DEG	DEG
	<i>Cyp2b1</i>	0.002		DEG	DEG	DEG	DEG	DEG	DEG	DEG
	<i>Ehhadh</i>	0.007			DEG	DEG	DEG	DEG	DEG	DEG
	<i>Abcg8</i>	0.009			DEG	DEG	DEG	DEG	DEG	DEG
	<i>Creb3l3</i>	0.012				DEG	DEG	DEG	DEG	DEG
	<i>B3galt1</i>	0.018				DEG	DEG	DEG	DEG	DEG
	<i>Ppap2b</i>	0.022				DEG	DEG	DEG	DEG	DEG
	<i>Gadd45b</i>	0.022				DEG	DEG	DEG	DEG	DEG
	<i>Upp2</i>	0.026				DEG	DEG	DEG	DEG	DEG
	<i>Xiap</i>	0.033				DEG	DEG	DEG	DEG	DEG
<i>Creb3l2</i>	0.047				DEG	DEG	DEG	DEG	DEG	

Table 2. q values from experimental parameter comparisons between the up-regulated and down-regulated IRGs by changing the Cuffdiff's internal threshold (FDR).

Parameter	FDR threshold							
	0.001	0.005	0.01	0.05	0.1	0.5	0.9	1
Time_Constant_Step	0.15	0.082	0.08	6.3×10 ^{-3*}				
Time_Peak_Pulse	0.21	0.093	0.028	0.071	0.071	0.071	0.071	0.071
Time_Decay_Pulse	0.035	0.021	1.6×10 ^{-3*}	1.1×10 ^{-3*}				
Ratio_240min_Pulse	6.9×10 ^{-3*}	3.7×10 ^{-3*}	4.4×10 ^{-4*}	2.5×10 ^{-3*}				
Time_Constant_Ramp	0.32	0.24	0.091	0.013	0.013	0.013	0.013	0.013
Ratio_120min_Ramp	0.15	0.082	0.15	0.015	0.015	0.015	0.015	0.015
Ratio_180min_Ramp	0.45	0.42	0.99	0.98	0.98	0.98	0.98	0.98
Ratio_240min_Ramp	0.45	0.42	0.76	0.86	0.86	0.86	0.86	0.86
Hill's coefficient(120 min)	0.012	6.2×10 ^{-3*}	7.3×10 ^{-3*}	1.7×10 ^{-3*}				
Hill's coefficient(240 min)	0.82	0.95	0.27	0.21	0.21	0.21	0.21	0.21
EC ₅₀ (120 min)	6.9×10 ^{-3*}	3.7×10 ^{-3*}	0.043	4.6×10 ^{-3*}				
EC ₅₀ (240 min)	6.9×10 ^{-3*}	3.7×10 ^{-3*}	4.4×10 ^{-4*}	9.1×10 ^{-5*}				
V _{max} (120 min)	6.9×10 ^{-3*}	3.7×10 ^{-3*}	2.5×10 ^{-3*}					
V _{max} (240 min)	6.9×10 ^{-3*}	3.7×10 ^{-3*}	4.4×10 ^{-4*}	1.7×10 ^{-3*}				
b (120 min)	0.082	0.044	0.038	2.5×10 ^{-3*}				
b (240 min)	0.63	0.89	1.0×10 ⁰	0.81	0.81	0.81	0.81	0.81

* q value < 0.01 after multiple testing correction based on Benjamini-Hochberg method (see Materials and Methods).

Table 3. KEGG pathways into which five or more IRGs mapped.

KEGG pathway name	KEGG pathway ID	Numbers of mapped IRGs
Metabolic pathways	rno01100	14
MAPK signaling pathway	rno04010	12
Bile secretion	rno04976	7
PI3K-Akt signaling pathway	rno04151	7
Estrogen signaling pathway	rno04915	6
Insulin signaling pathway	rno04910	6
Hippo signaling pathway	rno04390	6
p53 signaling pathway	rno04115	6
Focal adhesion	rno04510	6
TNF signaling pathway	rno04668	5
Cell cycle	rno04110	5
Ras signaling pathway	rno04014	5

Table 4. KEGG pathways in which the up-regulated and down-regulated IRGs were mapped.

Up-regulated IRGs	KEGG pathway(s)
<i>Actb</i>	Focal adhesion, Hippo signaling pathway
<i>Actg1</i>	Focal adhesion, Hippo signaling pathway
<i>Ajuba</i>	Hippo signaling pathway
<i>Epha2</i>	PI3K-Akt signaling pathway, Ras signaling pathway
<i>Gabbr1</i>	Estrogen signaling pathway
<i>Gadd45a</i>	Cell cycle, MAPK signaling pathway, p53 signaling pathway
<i>Hbegf</i>	Estrogen signaling pathway
<i>Hmgcr</i>	Metabolic pathways, bile secretion
<i>Mat2a</i>	Metabolic pathways
<i>Msmo1</i>	Metabolic pathways
<i>Rassf1</i>	Hippo signaling pathway, Ras signaling pathway
<i>Srf</i>	MAPK signaling pathway
<i>Zyx</i>	Focal adhesion

Down-regulated IRGs	KEGG pathway(s)
<i>Abcg8</i>	Bile secretion
<i>B3galt1</i>	Metabolic pathways
<i>Ccng2</i>	p53 signaling pathway
<i>Creb3l2</i>	Estrogen signaling pathway, PI3K-Akt signaling pathway, TNF signaling pathway
<i>Creb3l3</i>	Estrogen signaling pathway, PI3K-Akt signaling pathway, TNF signaling pathway
<i>Cyp2b1</i>	Metabolic pathways
<i>Ehhadh</i>	Metabolic pathways
<i>G6pase</i>	Insulin signaling pathway, metabolic pathways, PI3K-Akt signaling pathway
<i>Gadd45b</i>	Cell cycle, MAPK signaling pathway, p53 signaling pathway
<i>Irs2</i>	Insulin signaling pathway
<i>Lpin1</i>	Metabolic pathways
<i>Nr0b2</i>	Bile secretion
<i>Pck1</i>	Insulin signaling pathway, metabolic pathways, PI3K-Akt signaling pathway
<i>Ppap2b</i>	Metabolic pathways
<i>Upp2</i>	Metabolic pathways
<i>Xiap</i>	Focal adhesion

Table 5. Primer sequences used for qRT-PCR measurements.

Sustained increased IRGs	Forward	Reverse
<i>Actb</i> [†]	ACCAGTTCGCCATGGATGAC	TGCCGGAGCCGTTGTC
<i>Actg1</i> [†]	GAGTCAGGCCCTCCATTGT	GCCTGGCACCTGCTCAGT
<i>Ajuba</i> [†]	TGAGAGGGCATCACAGAAACC	GGCCAAGCTAACCCCTATGTGAA
<i>Cxcl1</i>	CAGACAGTGGCAGGGATTCA	CCTGGCGGCATCACCTT
<i>Dusp5</i>	CAGGGTGGCCCAGTTGAA	GATGCATGGTAGGCACTTCCA
<i>Epha2</i> [†]	GCATTGCTCTCTGTTCGTGTCT	GGAAGCGGGCCAAGCT
<i>Gabbr1</i> [†]	TCTCCATTCTGCCCCAGTTG	CATAGAAAATGCCAAGCCACGTA
<i>Gadd45a</i> [†]	TGGCTGCGGATGAAGATGA	CACGAATGAGGGTGAAATGGA
<i>Hbegf</i>	TCTTTCTGGCCGCAGTGTT	GAAGCCGCTCCAGACTCTCA
<i>Hmger</i> [†]	CTGGGCCCCACGTTCA	ATGGTGCCAACTCCAATCACA
<i>Mat2a</i> [†]	CTTGGTTACGCCCAGATTCTAAA	CACAGCACCTCGATCTTGCA
<i>Msmo1</i> [†]	TCACGATTTCCACCACATGAA	TGTCCCACCACGTGAAGGT
<i>Ppp1r3b</i>	GGACAGCAACAAAGGCAAAAAC	TTCCCTGGGTGGATCTGAGTT
<i>Ppp3r1</i>	CGGACTTGCAGTCACAGATTTTC	GAAGTGGTCTTTGCCTTTTTTCC
<i>Rassf1</i> [†]	CTGGAGCAGCACGACAAGTAGT	TGAAGTACTGCTCGAGCTCTGAGT
<i>Serpine1</i>	TCCGGATGGGCACGAGTA	GAGGGTTTCGCCGTGGTA
<i>Srf</i>	CACGACCTTCAGCAAGAGGAA	CAGCGTGGACAGCTCATAAGC
<i>Zyx</i> [†]	TGTCCTCACTGCTGGATGACA	TGACACCCGGGCTTTGA

[†]Up-regulated IRGs.

Sustained decreased IRGs	Forward	Reverse
<i>Abcg8</i> [‡]	CACCTACAGTGGTCAGTCCAACAC	CTCAAACCAAGGCACCTGAGA
<i>Amacr</i>	GGTCATTGATGCGAACATGGTGGAA	CCCATGGCTTGAGTTTTCCA
<i>B3galt1</i> [‡]	AATGGCGGGCCAATCAG	CAGGGTACAAATCCCTAGGCATA
<i>Cng2</i> [‡]	TCAGGAATGCACCTTCTTCTTTG	TGAACTCTAAGGTGGAAAGCACAGT
<i>Cflar</i>	GGGTGCGGCGGTTTG	CCACCGCTGCTTTATCTGTCT
<i>Creb3l2</i> [‡]	TGGTCGTTGTGCTTTGCTTT	GATACAGCCCGTAGCCTTGAAA
<i>Creb3l3</i> [‡]	TGGATCCGCTAACGTTGCA	GCCCCTCGCCTTGCTT
<i>Cyp2b1</i> [‡]	CCCCCATGTGCGCAGAGAA	CCGGTGTGAGCCGATCAC
<i>Ehhadh</i> [‡]	TCCGGGCAGGCTAAAGC	TGACCACTTATTTGCAGACTTTTCA
<i>G6pase</i> [‡]	CAGCCCGTGTAATGAGTAGC	GATGAGTCCTATGGCACGCAGACCT
<i>Gadd45b</i> [‡]	TGCTGGCCATAGACGAAGAA	ATCAGGGTGAAGTGAATTTGCA
<i>Irs2</i> [‡]	CAAGAACCTGACCGGTGTATAACC	GGCTGTTTCGCAATTGAGCTT
<i>Lpin1</i> [‡]	CCGTGTCATATCAGCAATTTGC	GACCACGAGGTTGGGATCAT
<i>Nr0b2</i> [‡]	CGCCTGGCCCGAATC	GAAGGGTACAGGAGATGTTCTTGAG
<i>Pck1</i> [‡]	CGCTATGCGGCCCTTCT	AGCCAGTGCGCCAGGTACT
<i>Ppap2b</i> [‡]	TTTTTCGGCTGTGCCATCA	GCGCCCAATGGACACTTT
<i>Upp2</i> [‡]	TGGTGGGAGCTCGAACAGA	AACCCGAGTTCCTTGTGCAT
<i>Xiap</i> [‡]	GCCCGCGGCGGTTA	AATACGACTTGTCCACCTTTTCG

[‡]Down-regulated IRGs.

Table 6. Parameters of the experimental IRG responses.

Stimulation	Parameter	Description
Step (Fig. 10A)	Time_Constant_Step	Time when the expression amount reached 1/2 Peak_Step
	Time_Peak_Pulse	Time when the expression amount reached Peak_Pulse
Pulse (Fig. 10A)	Time_Decay_Pulse	Time when the expression amount reached 1/2 Peak_Pulse after the time of Peak_Pulse
	Ratio_240min_Pulse	240min_Pulse / 240min_Step
Ramp (Fig. 10A)	Time_Constant_Ramp	Time when the expression amount reached 1/2 Peak_Ramp
	Ratio_120min_Ramp	120min_Ramp / 120min_Step
	Ratio_180min_Ramp	180min_Ramp / 180min_Step
	Ratio_240min_Ramp	240min_Ramp / 240min_Step
Dose-response (Fig. 10B)	Hill's coefficient, EC_{50} , V_{max} , and b	Each parameter was estimated at 120 and 240 min

Table 7. Up-regulated IRGs and down-regulated IRGs.

Up-regulated IRGs	Down-regulated IRGs
<i>Actb</i> *	<i>Abcg8</i>
<i>Actg1</i>	<i>B3galt1</i>
<i>Ajuba</i>	<i>Ccng2</i> †
<i>Epha2</i>	<i>Creb3l2</i>
<i>Gabbr1</i>	<i>Creb3l3</i>
<i>Gadd45a</i> †	<i>Cyp2b1</i>
<i>Hbegf</i>	<i>Ehhadh</i> †
<i>Hmgcr</i> †	<i>G6pase</i> *†
<i>Mat2a</i>	<i>Gadd45b</i>
<i>Msmo1</i> *	<i>Irs2</i> †
<i>Rassf1</i> *	<i>Lpin1</i>
<i>Srf</i> †	<i>Nr0b2</i>
<i>Zyx</i> *†	<i>Pck1</i> *†
	<i>Ppap2b</i>
	<i>Upp2</i>
	<i>Xiap</i>

*Up-regulated and down-regulated genes by insulin stimulation (100 nM for 6 hours) in rat H4IIE hepatoma cells (11). Note that the cell line and the time point are different from those of our study.

† Up-regulated and down-regulated IRGs by insulin injection in the liver (Fig. 9).

Table 8. Calculated parameters from experimental qRT-PCR data.

Up-regulated IRGs	Time_ Constant_ Step (min)	Time_ Peak_ Pulse (min)	Time_ Decay_ Pulse (min)	Ratio_ 240min_ Pulse	Time_ Constant_ Ramp (min)
<i>Actb</i>	6.27×10^1	2.40×10^2	2.40×10^2	3.80×10^{-1}	6.78×10^1
<i>Actg1</i>	5.87×10^1	1.20×10^2	2.40×10^2	2.04×10^{-1}	6.58×10^1
<i>Ajuba</i>	7.02×10^1	1.20×10^2	2.02×10^2	1.25×10^{-1}	6.54×10^1
<i>Epha2</i>	4.06×10^1	6.00×10^1	1.42×10^2	3.06×10^{-3}	5.77×10^1
<i>Gabbr1</i>	1.07×10^1	3.00×10^1	7.06×10^1	6.78×10^{-1}	4.11×10^1
<i>Gadd45a</i>	2.72×10^1	9.00×10^1	1.67×10^2	4.09×10^{-1}	1.83×10^1
<i>Hbegf</i>	2.38×10^1	6.00×10^1	1.03×10^2	4.20×10^{-2}	4.56×10^1
<i>Hmgcr</i>	3.54×10^1	1.20×10^2	1.78×10^2	6.67×10^{-1}	5.97×10^1
<i>Mat2a</i>	4.75×10^1	1.20×10^2	2.24×10^2	2.83×10^{-1}	4.87×10^1
<i>Msmo1</i>	7.07×10^1	1.20×10^2	1.88×10^2	0.00×10^0	8.87×10^1
<i>Rassf1</i>	3.91×10^1	6.00×10^1	1.43×10^2	2.15×10^{-1}	1.24×10^2
<i>Srf</i>	4.13×10^1	1.20×10^2	1.76×10^2	2.89×10^{-2}	5.40×10^1
<i>Zyx</i>	5.55×10^2	1.20×10^2	2.25×10^2	2.84×10^{-1}	6.56×10^1

Up-regulated IRGs	Ratio_ 120min_ Ramp	Ratio_ 180min_ Ramp	Ratio_ 240min_ Ramp	Hill's coefficient (120 min)	Hill's coefficient (240 min)
<i>Actb</i>	7.99×10^{-1}	8.47×10^{-1}	1.07×10^0	3.96×10^{-1}	7.88×10^{-1}
<i>Actg1</i>	1.09×10^0	1.00×10^0	9.59×10^{-1}	2.76×10^{-1}	7.31×10^{-1}
<i>Ajuba</i>	1.27×10^0	1.25×10^0	1.53×10^0	8.66×10^{-1}	6.60×10^{-1}
<i>Epha2</i>	1.28×10^0	1.60×10^0	1.24×10^0	2.90×10^{-1}	1.05×10^0
<i>Gabbr1</i>	0.00×10^0	1.12×10^0	1.59×10^{-1}	1.00×10^{-1}	1.00×10^1
<i>Gadd45a</i>	3.21×10^{-1}	5.67×10^{-1}	6.27×10^{-1}	2.64×10^{-1}	1.00×10^1
<i>Hbegf</i>	8.63×10^{-1}	1.23×10^0	1.03×10^0	2.74×10^{-1}	6.34×10^{-1}
<i>Hmgcr</i>	6.55×10^{-1}	1.08×10^0	1.74×10^0	1.42×10^{-1}	3.05×10^{-1}
<i>Mat2a</i>	1.29×10^0	1.20×10^0	1.37×10^0	9.34×10^{-1}	4.53×10^{-1}
<i>Msmo1</i>	1.21×10^0	1.16×10^0	1.44×10^0	1.36×10^{-1}	4.23×10^{-1}
<i>Rassf1</i>	9.25×10^{-1}	1.20×10^0	1.40×10^0	2.40×10^{-1}	3.59×10^0
<i>Srf</i>	6.42×10^{-1}	8.11×10^{-1}	7.56×10^{-1}	2.84×10^{-1}	6.44×10^{-1}
<i>Zyx</i>	7.60×10^{-1}	6.45×10^{-1}	5.94×10^{-1}	5.93×10^{-1}	1.31×10^0

Up-regulated IRGs	EC ₅₀ (nM) (120 min)	EC ₅₀ (nM) (240 min)	V _{max} (120 min)	V _{max} (240 min)	b (120 min)	b (240 min)
<i>Actb</i>	8.68×10 ⁻¹	1.30×10 ¹	1.30×10 ⁰	1.69×10 ⁰	9.89×10 ⁻¹	1.28×10 ⁰
<i>Actg1</i>	8.84×10 ¹	8.27×10 ⁰	4.36×10 ⁰	3.44×10 ⁰	5.79×10 ⁻¹	8.52×10 ⁻¹
<i>Ajuba</i>	2.42×10 ⁻¹	1.28×10 ¹	1.22×10 ⁰	2.16×10 ⁰	9.39×10 ⁻¹	1.11×10 ⁰
<i>Epha2</i>	1.00×10 ⁶	1.56×10 ¹	7.28×10 ¹	3.73×10 ⁰	9.56×10 ⁻¹	1.46×10 ⁰
<i>Gabbr1</i>	2.71×10 ⁰	1.33×10 ¹	2.52×10 ⁰	6.24×10 ⁻¹	7.46×10 ⁻¹⁰	1.02×10 ⁰
<i>Gadd45a</i>	1.00×10 ⁶	1.17×10 ¹	3.31×10 ¹	1.98×10 ⁰	7.27×10 ⁻¹	1.24×10 ⁰
<i>Hbegf</i>	1.00×10 ⁶	3.69×10 ¹	3.98×10 ¹	3.32×10 ⁰	7.77×10 ⁻¹	1.06×10 ⁰
<i>Hmgcr</i>	1.00×10 ⁶	1.00×10 ⁶	5.77×10 ⁰	1.50×10 ¹	7.99×10 ⁻¹	1.04×10 ⁰
<i>Mat2a</i>	1.10×10 ⁻¹	1.75×10 ⁰	9.27×10 ⁻¹	1.66×10 ⁰	8.36×10 ⁻¹	7.66×10 ⁻¹
<i>Msmo1</i>	7.26×10 ⁻³	7.30×10 ¹	1.77×10 ⁰	1.24×10 ⁰	1.04×10 ⁻⁹	9.05×10 ⁻¹
<i>Rassf1</i>	1.00×10 ⁶	1.50×10 ¹	2.14×10 ¹	1.50×10 ⁰	7.22×10 ⁻¹	1.21×10 ⁰
<i>Srf</i>	2.97×10 ²	2.83×10 ¹	6.55×10 ⁰	3.20×10 ⁰	5.52×10 ⁻¹	8.70×10 ⁻¹
<i>Zyx</i>	1.63×10 ¹	1.32×10 ¹	7.89×10 ⁰	5.72×10 ⁰	6.74×10 ⁻¹	7.83×10 ⁻¹

Down-regulated IRGs	Time_ Constant_ Step (min)	Time_ Peak_ Pulse (min)	Time_ Decay_ Pulse (min)	Ratio_ 240min_ Pulse	Time_ Constant_ Ramp (min)
<i>Abcg8</i>	1.07×10 ²	2.40×10 ²	2.40×10 ²	9.38×10 ⁻¹	1.42×10 ²
<i>B3galt1</i>	5.78×10 ¹	1.20×10 ²	1.73×10 ²	0.00×10 ⁰	7.23×10 ¹
<i>Ccng2</i>	3.55×10 ¹	1.20×10 ²	2.40×10 ²	6.04×10 ⁻¹	6.09×10 ¹
<i>Creb3l2</i>	1.09×10 ²	1.80×10 ²	2.40×10 ²	8.72×10 ⁻¹	9.28×10 ¹
<i>Creb3l3</i>	1.17×10 ²	2.40×10 ²	2.40×10 ²	9.06×10 ⁻¹	7.43×10 ¹
<i>Cyp2b1</i>	1.29×10 ²	1.80×10 ²	2.40×10 ²	5.85×10 ⁻¹	9.74×10 ¹
<i>Ehhadh</i>	5.95×10 ¹	1.80×10 ²	2.40×10 ²	4.07×10 ⁻¹	1.12×10 ²
<i>G6pase</i>	5.37×10 ¹	1.20×10 ²	2.37×10 ²	4.28×10 ⁻¹	5.81×10 ¹
<i>Gadd45b</i>	2.60×10 ¹	6.00×10 ¹	2.40×10 ²	6.70×10 ⁻¹	7.19×10 ¹
<i>Irs2</i>	6.07×10 ¹	9.00×10 ¹	2.40×10 ²	5.47×10 ⁻¹	8.17×10 ¹
<i>Lpin1</i>	6.82×10 ¹	1.20×10 ²	2.40×10 ²	5.05×10 ⁻¹	8.22×10 ¹
<i>Nr0b2</i>	8.77×10 ¹	1.80×10 ²	2.40×10 ²	7.10×10 ⁻¹	7.64×10 ¹
<i>Pck1</i>	9.24×10 ¹	1.80×10 ²	2.40×10 ²	8.27×10 ⁻¹	9.79×10 ¹
<i>Ppap2b</i>	9.17×10 ¹	9.00×10 ¹	2.40×10 ²	5.38×10 ⁻¹	1.66×10 ²
<i>Upp2</i>	8.54×10 ¹	1.80×10 ²	2.40×10 ²	7.60×10 ⁻¹	8.98×10 ¹
<i>Xiap</i>	1.10×10 ²	9.00×10 ¹	2.40×10 ²	8.42×10 ⁻¹	1.27×10 ¹

Down-regulated IRGs	Ratio_ 120min_ Ramp	Ratio_ 180min_ Ramp	Ratio_ 240min_ Ramp	Hill's coefficient (120 min)	Hill's coefficient (240 min)
<i>Abcg8</i>	1.53×10 ⁰	1.35×10 ⁰	1.15×10 ⁰	1.00×10 ¹	3.54×10 ⁰
<i>B3galt1</i>	1.17×10 ⁰	1.09×10 ⁰	1.14×10 ⁰	4.07×10 ⁻¹	4.64×10 ⁻¹
<i>Ccng2</i>	9.13×10 ⁻¹	1.00×10 ⁰	9.60×10 ⁻¹	3.26×10 ⁻¹	1.85×10 ⁰
<i>Creb3l2</i>	1.23×10 ⁰	9.76×10 ⁻¹	9.21×10 ⁻¹	1.00×10 ¹	3.62×10 ⁻¹
<i>Creb3l3</i>	1.20×10 ⁰	1.17×10 ⁰	1.09×10 ⁰	3.92×10 ⁻¹	1.89×10 ⁰
<i>Cyp2b1</i>	1.40×10 ⁰	1.14×10 ⁰	1.14×10 ⁰	1.03×10 ⁰	9.89×10 ⁻¹
<i>Ehhadh</i>	1.15×10 ⁰	1.12×10 ⁰	9.55×10 ⁻¹	1.62×10 ⁰	1.10×10 ⁰
<i>G6pase</i>	1.04×10 ⁰	1.01×10 ⁰	1.01×10 ⁰	7.32×10 ⁻¹	1.76×10 ⁰
<i>Gadd45b</i>	4.09×10 ¹	1.21×10 ¹	3.82×10 ⁰	3.78×10 ⁻¹	1.00×10 ¹
<i>Irs2</i>	1.38×10 ⁰	1.20×10 ⁰	1.17×10 ⁰	8.89×10 ⁻¹	2.58×10 ⁰
<i>Lpin1</i>	1.40×10 ⁰	1.07×10 ⁰	1.05×10 ⁰	1.15×10 ⁰	6.40×10 ⁻¹
<i>Nr0b2</i>	1.12×10 ⁰	1.05×10 ⁰	1.01×10 ⁰	7.58×10 ⁻¹	1.66×10 ⁰
<i>Pck1</i>	1.23×10 ⁰	1.06×10 ⁰	1.02×10 ⁰	2.27×10 ⁰	1.96×10 ⁰
<i>Ppap2b</i>	8.83×10 ⁻¹	9.84×10 ⁻¹	1.06×10 ⁰	1.00×10 ¹	1.12×10 ⁰
<i>Upp2</i>	1.44×10 ⁰	1.13×10 ⁰	1.06×10 ⁰	9.87×10 ⁻¹	2.19×10 ⁰
<i>Xiap</i>	9.05×10 ⁻¹	7.83×10 ⁻¹	8.14×10 ⁻¹	5.06×10 ⁻¹	2.06×10 ⁰

Down-regulated IRGs	EC ₅₀ (nM) (120 min)	EC ₅₀ (nM) (240 min)	V _{max} (120 min)	V _{max} (240 min)	<i>b</i> (120 min)	<i>b</i> (240 min)
<i>Abcg8</i>	5.10×10 ⁻¹	1.76×10 ⁻¹	1.42×10 ⁻¹	3.13×10 ⁻¹	6.83×10 ⁻¹	6.32×10 ⁻¹
<i>B3galt1</i>	6.05×10 ⁻¹	1.47×10 ⁻¹	1.72×10 ⁰	1.87×10 ⁰	2.12×10 ⁰	2.44×10 ⁰
<i>Ccng2</i>	5.90×10 ⁻⁵	1.41×10 ⁻¹	3.62×10 ⁰	5.20×10 ⁻¹	3.74×10 ⁰	7.13×10 ⁻¹
<i>Creb3l2</i>	4.14×10 ⁰	1.17×10 ⁻⁴	1.86×10 ⁻¹	4.78×10 ⁰	1.29×10 ⁰	5.56×10 ⁰
<i>Creb3l3</i>	1.77×10 ⁻⁶	1.33×10 ⁻¹	9.34×10 ⁰	5.54×10 ⁻¹	1.00×10 ⁻¹	9.79×10 ⁻¹
<i>Cyp2b1</i>	6.07×10 ⁻¹	1.59×10 ⁻¹	3.31×10 ⁻¹	8.68×10 ⁻¹	1.14×10 ⁰	1.26×10 ⁰
<i>Ehhadh</i>	1.53×10 ⁻¹	9.69×10 ⁻²	4.86×10 ⁻¹	1.02×10 ⁰	1.35×10 ⁰	1.91×10 ⁰
<i>G6pase</i>	7.34×10 ⁻²	1.72×10 ⁻¹	1.31×10 ⁰	1.27×10 ⁰	1.46×10 ⁰	1.42×10 ⁰
<i>Gadd45b</i>	3.23×10 ⁻⁶	1.10×10 ⁻¹	9.50×10 ⁰	2.05×10 ⁻¹	1.00×10 ⁻¹	7.23×10 ⁻¹
<i>Irs2</i>	1.33×10 ⁻¹	1.74×10 ⁻¹	4.33×10 ⁻¹	4.46×10 ⁻¹	8.65×10 ⁻¹	8.01×10 ⁻¹
<i>Lpin1</i>	6.44×10 ⁻²	4.97×10 ⁻²	5.69×10 ⁻¹	9.72×10 ⁻¹	9.58×10 ⁻¹	1.31×10 ⁰
<i>Nr0b2</i>	1.52×10 ⁻¹	1.24×10 ⁻¹	5.87×10 ⁻¹	7.80×10 ⁻¹	9.23×10 ⁻¹	9.76×10 ⁻¹
<i>Pck1</i>	8.12×10 ⁻²	9.93×10 ⁻²	3.52×10 ⁻¹	5.46×10 ⁻¹	6.99×10 ⁻¹	6.96×10 ⁻¹
<i>Ppap2b</i>	3.48×10 ⁰	1.77×10 ⁻¹	2.65×10 ⁻¹	6.00×10 ⁻¹	9.49×10 ⁻¹	1.18×10 ⁰
<i>Upp2</i>	1.50×10 ⁻¹	1.09×10 ⁻¹	6.66×10 ⁻¹	9.06×10 ⁻¹	1.39×10 ⁰	1.47×10 ⁰
<i>Xiap</i>	9.11×10 ⁻¹	1.87×10 ⁻¹	2.89×10 ⁻¹	3.32×10 ⁻¹	8.75×10 ⁻¹	9.19×10 ⁻¹

Table 9. Estimated model parameters and simulated EC₅₀ at 120 or 240 min for the up-regulated and down-regulated IRGs.

Up-regulated IRGs	k_1 (1/min)	K_{M1} (nM)	k_2 (1/min)	K_{M2} (nM)	V_{max1} (nM/min)	EC ₅₀ (nM) (120 min)	EC ₅₀ (nM) (240 min)
<i>Actb</i>	3.46×10^{-5}	4.59×10^0	2.25×10^5	2.32×10^{-7}	1.98×10^{-9}	1.06×10^0	1.97×10^0
<i>Actg1</i>	1.95×10^{-5}	7.96×10^0	1.59×10^5	8.08×10^{-6}	1.83×10^{-8}	2.30×10^0	5.40×10^0
<i>Ajuba</i>	1.88×10^{-4}	9.64×10^{-1}	2.80×10^0	1.25×10^{-6}	1.13×10^{-8}	2.21×10^{-1}	3.96×10^{-1}
<i>Epha2</i>	2.22×10^{-4}	3.22×10^0	6.07×10^4	7.50×10^{-7}	1.72×10^{-8}	4.56×10^{-1}	6.29×10^{-1}
<i>Gabbr1</i>	3.74×10^{-6}	7.70×10^3	2.58×10^2	2.00×10^4	6.53×10^4	2.08×10^1	2.09×10^1
<i>Gadd45a</i>	6.06×10^{-5}	3.36×10^5	6.06×10^5	1.08×10^{-5}	7.05×10^{-3}	2.83×10^0	2.83×10^0
<i>Hbegf</i>	1.48×10^{-4}	7.22×10^0	4.15×10^5	4.30×10^{-7}	2.03×10^{-8}	6.71×10^{-1}	8.20×10^{-1}
<i>Hmgcr</i>	2.77×10^{-4}	4.80×10^0	1.01×10^{-1}	1.64×10^{-7}	3.45×10^{-8}	2.18×10^{-1}	2.41×10^{-1}
<i>Mat2a</i>	3.98×10^{-4}	5.33×10^{-1}	4.44×10^1	7.45×10^{-7}	1.08×10^{-8}	1.09×10^{-1}	1.74×10^{-1}
<i>Msmo1</i>	1.20×10^{-4}	8.41×10^{-1}	1.28×10^{-1}	2.03×10^{-7}	1.64×10^{-9}	2.05×10^{-1}	4.12×10^{-1}
<i>Rassf1</i>	3.51×10^{-5}	9.97×10^1	1.64×10^4	2.47×10^{-7}	5.22×10^{-8}	2.88×10^0	3.06×10^0
<i>Srf</i>	1.74×10^{-5}	6.15×10^5	8.32×10^5	1.02×10^{-6}	6.40×10^{-4}	6.48×10^0	6.48×10^0
<i>Zyx</i>	3.47×10^{-5}	1.43×10^4	4.50×10^2	1.46×10^{-6}	1.32×10^{-5}	7.80×10^0	7.81×10^0
Down-regulated IRGs	k_1 (1/min)	K_{M1} (nM)	k_2 (1/min)	K_{M2} (nM)	V_{max1} (nM/min)	EC ₅₀ (nM) (120 min)	EC ₅₀ (nM) (240 min)
<i>Abcg8</i>	4.12×10^{-3}	1.42×10^{-1}	7.36×10^{-3}	7.04×10^{-5}	1.09×10^{-5}	9.35×10^{-3}	1.58×10^{-2}
<i>B3galt1</i>	2.12×10^{-2}	1.18×10^0	2.11×10^{-2}	2.97×10^{-0}	1.32×10^{-1}	3.04×10^{-1}	3.88×10^{-1}
<i>Ccng2</i>	1.10×10^{-2}	4.22×10^{-1}	6.29×10^{-2}	2.43×10^{-6}	1.94×10^{-7}	5.13×10^{-2}	5.61×10^{-2}
<i>Creb3l2</i>	3.44×10^{-2}	2.85×10^2	3.00×10^{-3}	5.77×10^{-7}	1.47×10^{-4}	2.17×10^{-2}	4.39×10^{-2}
<i>Creb3l3</i>	3.32×10^{-2}	3.90×10^5	4.72×10^{-3}	5.20×10^{-7}	2.23×10^{-1}	1.89×10^{-2}	3.36×10^{-2}
<i>Cyp2b1</i>	3.17×10^{-4}	5.57×10^{-1}	1.11×10^{-2}	1.93×10^{-7}	5.26×10^{-7}	5.80×10^{-2}	1.34×10^{-1}
<i>Ehhadh</i>	1.13×10^{-2}	9.69×10^{-1}	3.15×10^{-2}	1.42×10^{-2}	2.01×10^{-4}	3.07×10^{-1}	4.56×10^{-1}
<i>G6pase</i>	1.53×10^{-2}	2.00×10^0	2.17×10^{-2}	1.11×10^{-4}	2.40×10^{-5}	1.16×10^{-1}	1.41×10^{-1}
<i>Gadd45b</i>	1.29×10^{-2}	2.51×10^{-1}	5.56×10^1	1.25×10^4	2.11×10^2	9.49×10^{-2}	1.12×10^{-1}
<i>Irs2</i>	7.44×10^{-3}	2.60×10^{-1}	3.42×10^{-2}	4.51×10^4	1.16×10^3	5.19×10^{-2}	7.14×10^{-2}
<i>Lpin1</i>	9.65×10^{-3}	3.34×10^{-1}	2.36×10^{-2}	1.41×10^{-3}	5.35×10^{-5}	5.58×10^{-2}	7.86×10^{-2}
<i>Nr0b2</i>	5.53×10^{-3}	3.68×10^{-1}	1.81×10^{-2}	6.38×10^2	4.09×10^1	3.29×10^{-2}	4.83×10^{-2}
<i>Pck1</i>	2.26×10^{-3}	2.84×10^{-1}	1.40×10^{-2}	1.24×10^{-5}	2.64×10^2	1.26×10^{-2}	1.79×10^{-2}
<i>Ppap2b</i>	2.90×10^{-2}	7.23×10^0	3.40×10^{-3}	3.17×10^2	1.02×10^2	2.72×10^{-1}	6.62×10^{-1}
<i>Upp2</i>	3.68×10^{-3}	3.13×10^{-1}	2.05×10^{-2}	3.88×10^2	1.21×10^1	4.06×10^{-2}	6.53×10^{-2}
<i>Xiap</i>	3.57×10^{-2}	5.31×10^1	3.42×10^{-3}	3.58×10^{-7}	1.72×10^{-5}	2.24×10^{-2}	4.44×10^{-2}

7. References

1. A. R. Saltiel, C. R. Kahn, Insulin signalling and the regulation of glucose and lipid metabolism. *Nature* **414**, 799-806 (2001).
2. H. Yki-Jarvinen, Action of insulin on glucose metabolism *in vivo*. *Bailliere's Clin. Endocrinol. Metab.* **7**, 903-927 (1993).
3. J. R. Lindsay, A. M. McKillop, M. H. Mooney, P. R. Flatt, P. M. Bell, F. P. M. O'Harte, Meal-induced 24-hour profile of circulating glycated insulin in type 2 diabetic subjects measured by a novel radioimmunoassay. *Metabolism* **52**, 631-635 (2003).
4. K. S. Polonsky, B. D. Given, E. Vancauter, 24-hour profiles and pulsatile patterns of insulin-secretion in normal and obese subjects. *J. Clin. Invest.* **81**, 442-448 (1988).
5. D. G. Bruce, D. J. Chisholm, L. H. Storlien, E. W. Kraegen, Physiological importance of deficiency in early prandial insulin secretion in non-insulin-dependent diabetes. *Diabetes* **37**, 736-744 (1988).
6. S. Del Prato, Loss of early insulin secretion leads to postprandial hyperglycaemia. *Diabetologia* **46 Suppl 1**, M2-8 (2003).
7. R. E. Pratley, C. Weyer, The role of impaired early insulin secretion in the pathogenesis of Type II diabetes mellitus. *Diabetologia* **44**, 929-945 (2001).
8. H. Kubota, R. Noguchi, Y. Toyoshima, Y. Ozaki, S. Uda, K. Watanabe, W. Ogawa, S. Kuroda, Temporal coding of insulin action through multiplexing of the AKT pathway. *Mol.*

- Cell* **46**, 820-832 (2012).
9. R. Noguchi, H. Kubota, K. Yugi, Y. Toyoshima, Y. Komori, T. Soga, S. Kuroda, The selective control of glycolysis, gluconeogenesis and glycogenesis by temporal insulin patterns. *Mol. Syst. Biol.* **9**, 664 (2013).
 10. K. Yugi, H. Kubota, Y. Toyoshima, R. Noguchi, K. Kawata, Y. Komori, S. Uda, K. Kunida, Y. Tomizawa, Y. Funato, H. Miki, M. Matsumoto, K. I. Nakayama, K. Kashikura, K. Endo, K. Ikeda, T. Soga, S. Kuroda, Reconstruction of insulin signal flow from phosphoproteome and metabolome data. *Cell Rep.* **8**, 1171-1183 (2014).
 11. S. Tay, J. J. Hughey, T. K. Lee, T. Lipniacki, S. R. Quake, M. W. Covert, Single-cell NF-kappaB dynamics reveal digital activation and analogue information processing. *Nature* **466**, 267-271 (2010).
 12. S. Hao, D. Baltimore, RNA splicing regulates the temporal order of TNF-induced gene expression. *Proc Natl Acad Sci U S A* **110**, 11934-11939 (2013).
 13. G. G. Zampar, A. Kummel, J. Ewald, S. Jol, B. Niebel, P. Picotti, R. Aebersold, U. Sauer, N. Zamboni, M. Heinemann, Temporal system-level organization of the switch from glycolytic to gluconeogenic operation in yeast. *Mol Syst Biol* **9**, 651 (2013).
 14. T. L. Hectors, C. Vanparys, A. Pereira-Fernandes, D. Knapen, R. Blust, Mechanistic evaluation of the insulin response in H4IIE hepatoma cells: new endpoints for toxicity testing? *Toxicol. Lett.* **212**, 180-189 (2012).

15. J. Dupont, J. Khan, B. H. Qu, P. Metzler, L. Helman, D. LeRoith, Insulin and IGF-1 induce different patterns of gene expression in mouse fibroblast NIH-3T3 cells: identification by cDNA microarray analysis. *Endocrinology* **142**, 4969-4975 (2001).
16. S. Versteyhe, B. Klaproth, R. Borup, J. Palsgaard, M. Jensen, S. G. Gray, P. De Meyts, IGF-I, IGF-II, and insulin stimulate different gene expression responses through binding to the IGF-I receptor. *Front. Endocrinol.* **4**, 98 (2013).
17. H. S. Kim, N. K. Lee, Gene expression profiling in osteoclast precursors by insulin using microarray analysis. *Mol. Cells* **37**, 827-832 (2014).
18. S. Rome, K. Clement, R. Rabasa-Lhoret, E. Loizon, C. Poitou, G. S. Barsh, J. P. Riou, M. Laville, H. Vidal, Microarray profiling of human skeletal muscle reveals that insulin regulates not similar to 800 genes during a hyperinsulinemic clamp. *J. Biol. Chem.* **278**, 18063-18068 (2003).
19. L. Lassance, M. Haghiac, P. Leahy, S. Basu, J. Minium, J. Zhou, M. Reider, P. M. Catalano, S. Hauguel-De Mouzon, Identification of early transcriptome signatures in placenta exposed to insulin and obesity. *Am. J. Obstet. Gynecol.* **212**, 647.e641-e611 (2015).
20. M. Behar, D. Barken, S. L. Werner, A. Hoffmann, The dynamics of signaling as a pharmacological target. *Cell* **155**, 448-461 (2013).
21. M. Behar, A. Hoffmann, Understanding the temporal codes of intra-cellular signals. *Curr. Opin. Genet. Dev.* **20**, 684-693 (2010).

22. J. E. Purvis, G. Lahav, Encoding and decoding cellular information through signaling dynamics. *Cell* **152**, 945-956 (2013).
23. A. J. Lange, D. Argaud, M. R. Elmaghrabi, W. S. Pan, S. R. Maitra, S. J. Pilgis, Isolation of a Cdna for the Catalytic Subunit of Rat-Liver Glucose-6-Phosphatase - Regulation of Gene-Expression in Fao Hepatoma-Cells by Insulin, Dexamethasone and Camp. *Biochem Bioph Res Co* **201**, 302-309 (1994).
24. K. Matsumoto, A. Suzuki, H. Wakaguri, S. Sugano, Y. Suzuki, Construction of mate pair full-length cDNAs libraries and characterization of transcriptional start sites and termination sites. *Nucleic Acids Res.* **42**, e125 (2014).
25. C. Trapnell, A. Roberts, L. Goff, G. Pertea, D. Kim, D. R. Kelley, H. Pimentel, S. L. Salzberg, J. L. Rinn, L. Pachter, Differential gene and transcript expression analysis of RNA-seq experiments with TopHat and Cufflinks. *Nat. Protoc.* **7**, 562-578 (2012).
26. C. Trapnell, L. Pachter, S. L. Salzberg, TopHat: discovering splice junctions with RNA-Seq. *Bioinformatics* **25**, 1105-1111 (2009).
27. C. Trapnell, B. A. Williams, G. Pertea, A. Mortazavi, G. Kwan, M. J. van Baren, S. L. Salzberg, B. J. Wold, L. Pachter, Transcript assembly and quantification by RNA-Seq reveals unannotated transcripts and isoform switching during cell differentiation. *Nat. Biotechnol.* **28**, 511-515 (2010).
28. N. Otsu, A threshold selection method from gray-level histograms. *IEEE Trans. Syst., Man,*

- Cyber.* **9**, 62-66 (1979).
29. H. Ogata, S. Goto, K. Sato, W. Fujibuchi, H. Bono, M. Kanehisa, KEGG: Kyoto Encyclopedia of Genes and Genomes. *Nucleic Acids Res.* **27**, 29-34 (1999).
 30. R. J. Kinsella, A. Kahari, S. Haider, J. Zamora, G. Proctor, G. Spudich, J. Almeida-King, D. Staines, P. Derwent, A. Kerhornou, P. Kersey, P. Flicek, Ensembl BioMarts: a hub for data retrieval across taxonomic space. *Database (Oxford)* **2011**, bar030 (2011).
 31. J. C. Lagarias, J. A. Reeds, M. H. Wright, P. E. Wright, Convergence properties of the Nelder-Mead simplex method in low dimensions. *Siam J. Optimiz.* **9**, 112-147 (1998).
 32. Y. Benjamini, Y. Hochberg, Controlling the False Discovery Rate - a Practical and Powerful Approach to Multiple Testing. *J Roy Stat Soc B Met* **57**, 289-300 (1995).
 33. S. Hoops, S. Sahle, R. Gauges, C. Lee, J. Pahle, N. Simus, M. Singhal, L. Xu, P. Mendes, U. Kummer, COPASI-a COMplex PATHway SIMulator. *Bioinformatics* **22**, 3067-3074 (2006).
 34. A. V. Matveyenko, D. Liuwantara, T. Gurlo, D. Kirakossian, C. Dalla Man, C. Cobelli, M. F. White, K. D. Copps, E. Volpi, S. Fujita, P. C. Butler, Pulsatile portal vein insulin delivery enhances hepatic insulin action and signaling. *Diabetes* **61**, 2269-2279 (2012).
 35. H. Thorvaldsdottir, J. T. Robinson, J. P. Mesirov, Integrative Genomics Viewer (IGV): high-performance genomics data visualization and exploration. *Brief Bioinform* **14**, 178-192 (2013).
 36. S. Maere, K. Heymans, M. Kuiper, BiNGO: a Cytoscape plugin to assess overrepresentation

- of gene ontology categories in biological networks. *Bioinformatics* **21**, 3448-3449 (2005).
37. J. Twisk, M. F. Hoekman, E. M. Lehmann, P. Meijer, W. H. Mager, H. M. Princen, Insulin suppresses bile acid synthesis in cultured rat hepatocytes by down-regulation of cholesterol 7 alpha-hydroxylase and sterol 27-hydroxylase gene transcription. *Hepatology* **21**, 501-510 (1995).
38. E. Plagnes-Juan, M. Lansard, I. Seiliez, F. Medale, G. Corraze, S. Kaushik, S. Panserat, S. Skiba-Cassy, Insulin regulates the expression of several metabolism-related genes in the liver and primary hepatocytes of rainbow trout (*Oncorhynchus mykiss*). *J. Exp. Biol.* **211**, 2510-2518 (2008).
39. Y. Zhang, W. Chen, R. Li, Y. Li, Y. Ge, G. Chen, Insulin-regulated *Srebp-1c* and *Pck1* mRNA expression in primary hepatocytes from Zucker fatty but not lean rats is affected by feeding conditions. *PLoS One* **6**, e21342 (2011).
40. Y. Toyoshima, H. Kakuda, K. A. Fujita, S. Uda, S. Kuroda, Sensitivity control through attenuation of signal transfer efficiency by negative regulation of cellular signalling. *Nat. Commun.* **3**, 743 (2012).
41. L. S. Sidossis, R. R. Wolfe, Glucose and insulin-induced inhibition of fatty acid oxidation: the glucose-fatty acid cycle reversed. *Am J Physiol* **270**, E733-738 (1996).
42. Y. X. Sun, Y. Q. Zhang, N. Li, H. Zhang, L. B. Zhou, L. Shao, Exposure to high levels of glucose increases the expression levels of genes involved in cholesterol biosynthesis in rat

islets. *Exp. Ther. Med.* **8**, 991-997 (2014).

43. N. G. Gokey, C. Lopez-Anido, A. L. Gillian-Daniel, J. Svaren, Early growth response 1 (Egr1) regulates cholesterol biosynthetic gene expression. *J. Biol. Chem.* **286**, 29501-29510 (2011).
44. S. J. Humphrey, S. B. Azimifar, M. Mann, High-throughput phosphoproteomics reveals in vivo insulin signaling dynamics. *Nat Biotechnol* **33**, 990-995 (2015).

8. Acknowledgements

I thank all the members in Kuroda Laboratory for their critical reading of this manuscript; Y. Toyoshima for advice on estimation of parameters of dose-response curves; and R. Kuribayashi, S. Takizawa, and N. Matsuda for their technical assistances with the experiments. The computational analysis of this work was performed with partial support from the super computer system of the National Institute of Genetics Research Organization of Information and Systems. I am also deeply grateful to my family for plenty of physical, mental, and economical support.

This work was supported by the Creation of Fundamental Technologies for Understanding and Control of Biosystem Dynamics, CREST from the Japan Science and Technology Agency (JST); by the Japan Diabetes Foundation; by the Ono Medical Research Foundation; by the Japan Society for the Promotion of Science (JSPS) [JSPS Grants-in-Aid for Scientific Research (KAKENHI) grant no. JP15H05582] and by the “Creation of Innovative Technology for Medical Applications Based on the Global Analyses and Regulation of Disease-Related Metabolites,” PRESTO from JST; by “Elucidation and regulation in the dynamic maintenance and transfiguration of homeostasis in living body,” PRESTO from JST.

The sequencing data measured in this study have been deposited in the DNA Data Bank of Japan Sequence Read Archive (DRA) (www.ddbj.nig.ac.jp/) under the accession no. DRA004341. All other data are available with the published article. Supplementary data files S1-S8 can be downloaded from <http://stke.sciencemag.org/content/9/455/ra112>.